Lithos 320–321 (2018) 118–133

Contents lists available at ScienceDirect

Lithos

journal homepage: www.elsevier.com/locate/lithos

The petrogenesis of albitized Early-Permian trachyandesites from Świerki quarry (Lower Silesia, Poland) - constraints on spilitization supported by mineralogical and geochemical data

Tomasz Powolny [a,*], Magdalena Dumańska-Słowik [a], Magdalena Sikorska-Jaworowska [b]

[a] Department of Mineralogy, Petrography, and Geochemistry, Faculty of Geology, Geophysics, and Environmental Protection, AGH - University of Science and Technology, 30 Mickiewicza Av., Krakow 30-059, Poland
[b] Polish Geological Institute, National Research Institute, 4 Rakowiecka St., 00-975 Warsaw, Poland

ARTICLE INFO

Article history:
Received 7 March 2018
Accepted 31 August 2018
Available online 5 September 2018

Keywords:
Spilite
Metasomatism
Feldspar
Intra-Sudetic basin
Albitization
Zonal apatite
Al-O$^-$-Ti/Al-O$^-$-Al centres
Dissolution-reprecipitation mechanism

ABSTRACT

Trachyandesites from Świerki quarry (Lower Silesia, Poland), related to the post-collisional extension-related magmatic activity developed within the Intra-Sudetic Basin during Early-Permian times, are well-known for the occurrence of mineral associations typical of spilites (low-grade metamorphic rocks affected by Na-metasomatism). This paper deals with the reconstruction of the evolution of these rocks and puts constraints on the spilitization mechanism and its role in redistributing main and trace elements based on cathodoluminescence microscopy and spectroscopy combined with electron microprobe analysis. Our study reveals that the trachyandesites were strongly affected by low-temperature albitization, which occurred during the post-magmatic stage of the rock formation. The replacement of primary green luminescent andesine-labradorite ($An_{39-50}Ab_{47-58}Or_{2-3}$) by weakly-luminescent to dark-brown luminescent secondary albite (Ab~99 mol.%) was related to the CO_2-induced, crystallographically-controlled, interface-coupled dissolution-reprecipitation mechanism, triggered by hydraulic fracturing of fluids and/or contractional cooling forces. The replacive albite forms isolated and homogenous patches along polysynthetic twinning planes of andesine-labradorite and/or within intergranular fractures. It is closely associated with such minerals as calcite, chlorite and kaolinite, and exhibits enhanced microporosity. Moreover, the low-temperature alteration was accompanied by physicochemical fluctuations (alkaline-acidic) during rock formation as revealed by two generations of fluoroapatite: (1) violet-pink (REE^{3+}-activated) overprinted by (2) yellowish (Mn^{2+}-activated) luminescent domains. We also report that primary (green luminescent) plagioclases (andesine-labradorite) are rimmed by bright-blue luminescent Ab-rich ($An_{2-7}Ab_{34-61}Or_{32-64}$) alkali-feldspars followed by dull-blue luminescent Or-rich alkali-feldspars ($An_2Ab_{38-44}Or_{54-60}$). The bright-blue luminescent crystals contain higher amounts of BaO (~0.59 wt.%) and TiO_2 (~0.08 wt.%) than the dull-blue luminescent domains (~0.12 and 0.03 wt.%, respectively). Hence, the difference in CL intensity in blue wavelengths are ascribed to the presence of both Al-O$^-$-Al centres, related to a coupled KSi-BaAl substitution, and Al-O-Ti bridges. Not only the geochemical affinities of the rocks are peculiar to those reported for within-plate basalts, but also reveal similarities with arc-related geotectonic environments. Trachyandesites sourced from enriched subcontinental lithospheric mantle source owing to the strong LREE and LILE enrichment relative to Nb and Ta, while the presence of positive Zr—Hf anomalies coupled with low Nb/U ratios points to the involvement of crustal material during magma evolution. The spilitization has predominately resulted in the increase of Cs and decrease of Sr concentration among strongly-altered samples, while its influence on REE distribution was insignificant.

1. Introduction

Spilite is a venerable term for calcite-enriched basaltic rocks, which was first introduced by Brongniart (1827). Nowadays, it refers to a basic or intermediate (subvolcanic or volcanic), low-grade metamorphic rock in which the feldspar-group minerals are partially or almost entirely composed of albite accompanied by such minerals as chlorite, calcite, epidote, and/or prehnite (Árkai et al., 2007). Spilitization processes are strictly related to Na-metasomatism since spilitic rocks may contain significant amounts of albitized plagioclases forming as a result of the, variably defined, "spilite reaction". This reaction may be expressed by such an equation as: 2 $CaAl_2Si_2O_8$ (anorthite) + Na_2O + 2 SiO_2 → 2 $NaAlSi_3O_8$ (albite) +2 CaO + Al_2O_3 (Eskola

* Corresponding author.
E-mail address: powolny@agh.edu.pl (T. Powolny).

https://doi.org/10.1016/j.lithos.2018.08.037
0024-4937/

et al., 1937; Turner, 1948). The exact models of spilite formation have been debated for many years and were briefly summarized by Amstutz (1974). The specific mineral assemblages in spilitic rocks was of a primary magmatic origin and might either develop due to the direct crystallization from H_2O/Na_2O-enriched magma type or arise from the mixing of magma and hot brines (Lehmann, 1974a, 1974b; Xia et al., 1991). However, that theory has been almost completely abandoned these days. On the contrary, some authors (e.g. Vozár, 1974) proposed that the origin of spilites was strictly connected with late-magmatic, auto-metamorphic, or auto-metasomatic processes. Spilites may be also classified as low-grade metavolcanites altered during regional diagenetic burial metamorphism as well as post-magmatic hydrothermal processes (Mengel et al., 1987; Smith, 1968). The origin of the latter is sometimes assigned to water-rock interactions capable of providing a necessary source of Na^+ (e.g. Coombs, 1974; Munhá and Kerrich, 1980). Additionally, according to Hall (1990), sea-floor spilitization is associated with Mn-mineralization. Regardless of the model of spilitic rocks formation, the determination of primary magma or tectonic environment for these rock types may be difficult, because alteration processes are able to strongly affect both main and trace element composition (e.g. Floyd, 1977; Garcia, 1978; Hellman et al., 1979). One of the well-known occurrences of albitized volcanic rocks is the closed Świerki quarry located in the vicinity of Nowa Ruda (Lower Silesia, Poland).

A detailed petrographical description of these rocks was given by Dziedzicowa (1958), who noted that auto-hydrothermal alterations, including chloritization, uralitization, carbonatization, and albitization led to the formation of mineral assemblages typical of spilitic rocks. Nevertheless, the exact nature and origin of these rocks have remained not completely understood.

In this paper we present new mineralogical and petrological data for albitized Early-Permian trachyandesites from Świerki quarry based on optical microscopy, cathodoluminescence microscopy (OM-CL) and spectroscopy, scanning electron microscopy with energy dispersive spectrometry (SEM-EDS), and electron microprobe analysis (EMPA). The obtained results were used to reconstruct the multi-stage formation of these rocks and the mechanisms of albitization of plagioclases, related to fluctuations of physicochemical conditions during magma cooling and post-magmatic alterations. Based on bulk-rock major and trace element data, we determined the tectonic environment and revealed a possible role of low-grade metamorphic processes (spiltization) in the redistribution of elements - especially LREE (light rare earth elements) and LILE (large ion lithophile elements). The role of $Al\text{-}O^-$-Ti and $Al\text{-}O^-$-Al centres for the activation of blue luminescence colours among alkali-feldspars found within the rock matrix was also discussed.

2. Geological background

Świerki quarry is situated ca. 7 km N-W of Nowa Ruda in southwestern Poland (Fig. 1). It is divided into two parts including the so-called old (southern) and new (northern) one that had been providing a material for both construction industry and highway engineering before they were finally closed in 2012. The quarry is situated within the Intra-Sudetic basin, which represents a late Paleozoic intramontane trough infilled with Lower Permian and Lower Carboniferous sedimentary and volcanic rocks (e.g. Holub, 1976). The crystalline basement of the basin is composed of metamorphosed and deformed Precambrian or Paleozoic rocks (Franke and Żelaźniewicz, 2000). The Intra-Sudetic basin is located at the NE margin of the Bohemian Massif, between the crystalline massifs of the Karkonosze Mts., the Orlické Mts., the Bystřické Mts., and the Sowie Mts. It forms a synclinorial, fault-bounded structure, which stretches for around 60 km to WNW-ESE direction (Awdankiewicz et al., 2003; Holub, 1976; Lorenz and Nicholls, 1976; Wojewoda and Mastalerz, 1989).

The volcanic rocks exposed in Świerki quarry belong to the first volcanic cycle of the Middle Rotliegende (Kozłowski, 1963) and formed during the so-called subsequent Permian magmatic activity developed in Central Europe at the end of the Variscan orogeny. This type of magmatic activity was marked by cyclic re-occurrences of basic to acidic magmatic episodes and developed in subsidence-related areas, such as the Intra-Sudetic Basin (Kozłowski, 1963; McCann, 2008; Stille, 1950). The distribution of volcanoes and magma feeders was strictly linked to basin margins as well as intrabasinal elevations and their boundary faults (Awdankiewicz et al., 2003; Kozłowski, 1958). Therefore, Permian volcanogenic rocks from the Intra-Sudetic basin were generally emplaced within distinctive post-collisional, non-orogenic, and extension related settings (Awdankiewicz, 1999a, 1999b). Most of them are also commonly interlayered with clastic sediments (clayey shales) whose presence reflect the temporary lack of magmatic activity. These sediments were locally subjected to hydrothermal post-magmatic activity resulting in the silification of claystones (Awdankiewicz, 2004; Heflik and Pawlikowski, 1977).

The Świerki quarry is situated on a magmatic body whose genesis is currently not entirely understood. According to Kozłowski (1958, 1963), the eruptives represent near-surface top portions of great lava flows characterised by a thickness amounting to at most ca. 90 m. This observation arose from the fact that magmatic bodies exhibit specific loaf-like shape, as revealed in cross-sections, while rocks from the upper parts of the quarry are characterised by amygdaloidal textures. The rocks partially sank into underlying sediments (so-called building sandstones), which were consequently deformed and uplifted (Kozłowski, 1958, 1963). In contrast, Birkenmajer et al. (1968) considered the spilitic rocks from Świerki quarry to be a laccolith-type intrusion rather than extrusions. This statement may be further supported by the presence of thermally altered country rocks (mostly shales) and lack of structures typical to lava flow (Birkenmajer et al., 1968). Another possibility is that Permian extrusives from Świerki quarry extruded into a basin filled with water during early stage of its evolution (Dziedzic, 1958).

3. Sampling and analytical techniques

30 representative samples of volcanic rocks were investigated in this study. Samples were collected from the 2nd, 3rd, and 4th exploitation levels of the closed new quarry as well as from the lower levels of the old quarry.

3.1. Polarized light microscopy

Polished thin section were investigated using an Olympus BX51 polarizing microscope with a magnification range from 40 to 400 times. The photomicrographs were taken using an Olympus DP12 digital camera linked to Analysis software.

3.2. Scanning electron microscopy coupled with energy-dispersive X-ray spectrometry (SEM-EDS)

Back-scattered electron (BSE) observations were conducted on polished thin sections using a FEI Quanta 200 FEG scanning electron microscope equipped with an EDAX energy dispersive spectrometer (EDS) located at the Faculty of Geology, Geophysics and Environmental Protection AGH. The system operated at 25 kV accelerating voltage, 50 μA current, in a high-vacuum mode, i.e. 6×10^{-5}-7×10^{-6} Torr.

3.3. Electron microprobe analyses (EMPA) and WDXS elemental mapping

Electron-microprobe analyses were made at the Laboratory of Critical Elements of AGH University of Science and Technology – KGHM Polska Miedź S.A. using a JEOL Super Probe JXA-8230.The system operated

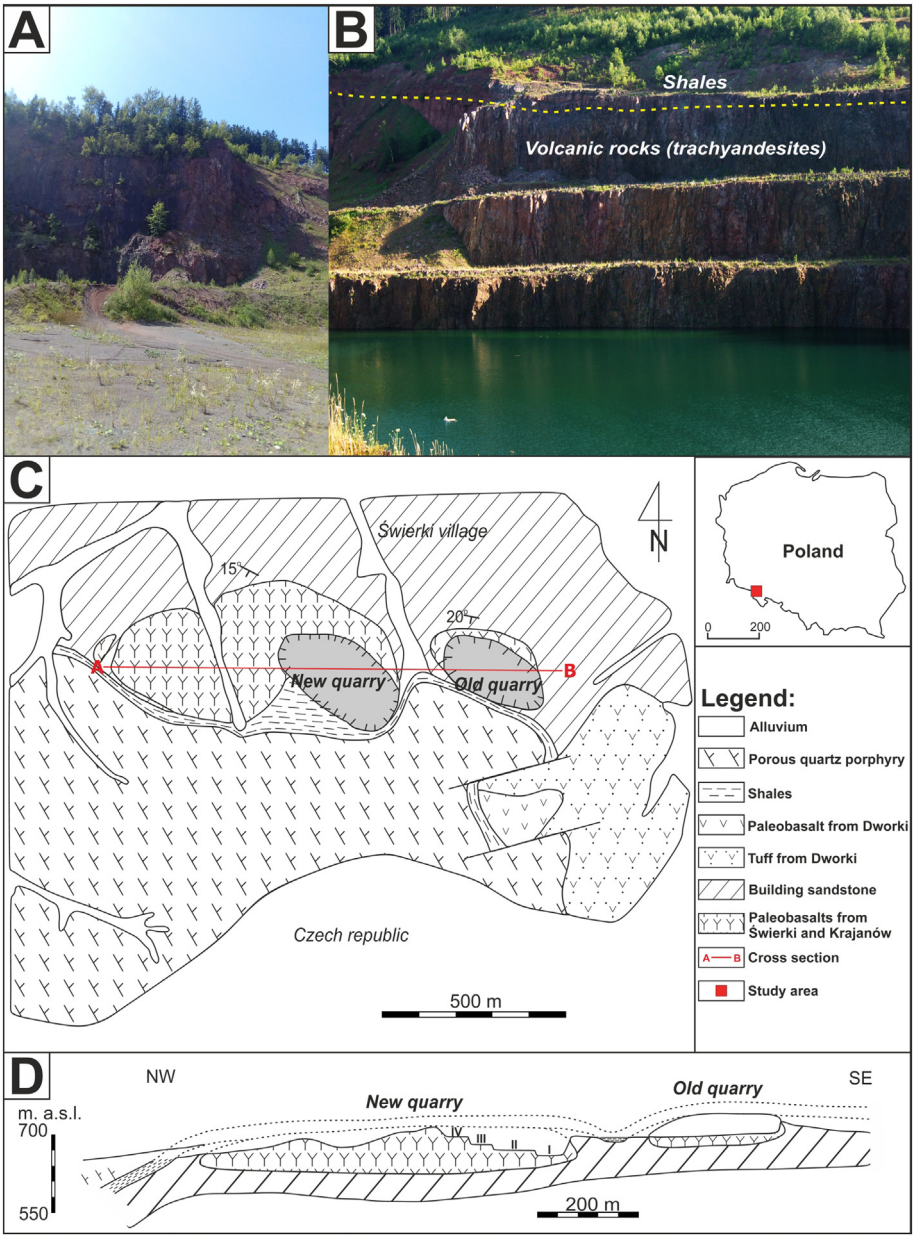

Fig. 1. Geological situation in the area of the study. (A, B) Field photo of old (A) and new (B) Świerki quarry with contact between magmatic rocks and overlying sediments (clay shales); (C) Geological map of the vicinity of Świerki village (modified after Kozłowski, 1958); (D) Geological cross-section (A-B) of the magmatic bodies from Świerki quarry (modified after Kozłowski, 1958); symbols I-IV refer to exploitation levels.

in a wavelength-dispersive (WDS) mode under the following conditions: accelerated voltage of 15 kV, beam current of 10 nA, peak count-time of 10 s, and background time of 5 s. The JEOL ZAF procedure was used for the matrix correction of the raw data. Standards, analytical lines, diffracting crystals and mean detection limits (wt%) were as follow: albite - Na (Kα, TAPH, 0.004), kyanite - Al (Kα, TAP, 0.004), albite - Si (Kα, TAP, 0.007), wollastonite - Ca (Kα, PETJ, 0.004), orthoclase - K (Kα, PETJ, 0.003), hematite - Fe (Kα, LIF, 0.015), MnO–Mn (Kα, LIFH, 0.005), forsterite - Mg (Kα, TAPH, 0.004), apatite - P (Kα, PETJ, 0.009), rutile - Ti (Kα, LIFL, 0.007), barite - Ba (Lα, PETL, 0.005), SrSO4 - Sr (Lα, PETL, 0.007). Overlap correction were performed on the basis of measured intensities and concentrations of interfering elements in the case of Ti (Kα - 4.510 keV) and Ba (Lα - 4467 keV). Correction coefficients were established as 0.01623 and 0.00435 for Ti and Ba, respectively. Compositional WDXS maps in a 150 μm × 165 μm area were acquired using an accelerating voltage of 15 kV, beam current of 10 nA, and dwell time of 250 ms. A step size was set as 0.5 μm. The results of the EMP analyses of feldspars combined with their CL characteristics are presented in Tables 1, 2, and 3. The crystal-chemical formulae of feldspars were normalized to contain 8 oxygen atom per formula unit.

3.4. Cathodoluminescence microscopy and spectroscopy

The cathodoluminescence analyses were conducted at the Polish Geological Institute - National Research Institute in Warsaw. The CL observations were performed on polished thin sections using a Cambridge Image Technology CCL 8200 MK3 device (cold cathode), coupled with a Nikon Optiphot 2 polarizing microscope, and equipped with a digital Canon EOS 600D camera. The scanning electron microscopy with cathodoluminescence (SEM-CL) analyses utilised a LEO 1430 scanning electron microscope coupled with a CL-image system (ASK-CL VIS

Table 1
Representative electron microprobe analyses of green luminescent plagioclases.

Location	New quarry			
	3rd exp. level			4th exp. level
CL colours	Greenish	Greenish	Grayish-green	Greenish
Special features	Primary hypidiomorphic crystals (weakly altered to albite)			Relicts surrounded by replacive albite
wt%				
SiO_2	53.54	54.63	54.31	56.52
TiO_2	0.08	0.09	0.07	0.09
Al_2O_3	27.33	27.45	27.05	25.78
Fe_2O_3	0.69	0.68	0.51	0.76
MnO	0.00	0.04	0.00	0.00
MgO	0.06	0.06	0.03	0.03
CaO	10.25	9.75	9.52	7.86
BaO	0.04	0.07	0.11	0.07
Na_2O	5.39	5.33	5.60	6.46
K_2O	0.53	0.45	0.39	0.56
Total	97.91	98.54	97.60	98.13
Formula based on O = 8				
Si	2.48	2.50	2.51	2.59
Ti	0.00	0.00	0.00	0.00
Al	1.49	1.48	1.47	1.39
Cr	0.00	0.00	0.00	0.00
Fe3	0.02	0.02	0.02	0.03
Fe2	0.00	0.00	0.00	0.00
Mn	0.00	0.00	0.00	0.00
Mg	0.00	0.00	0.00	0.00
Ca	0.51	0.48	0.47	0.39
Ba	0.00	0.00	0.00	0.00
Na	0.48	0.47	0.50	0.57
K	0.03	0.03	0.02	0.03
Cation sum	5.02	4.99	5.00	5.00
End member proportions				
An	49.66	48.94	47.29	38.85
Ab	47.26	48.38	50.38	57.84
Or	3.08	2.68	2.32	3.32

Table 2
Representative electron microprobe analyses of bright-blue luminescent and dull-blue luminescent alkali-feldspars.

Location	New quarry (3rd exp. level)							
CL colours	Bright-blue				Dull-blue			
Special features	Developed around green luminescent plagioclase				Developed between bright-blue luminescent feldspar and quartz			
wt%								
SiO_2	63.91	63.46	63.71	64.26	63.75	64.94	64.23	63.93
TiO_2	0.09	0.09	0.05	0.09	0.02	0.04	0.03	0.03
Al_2O_3	20.03	20.29	18.78	19.83	19.00	18.92	19.10	19.08
Fe_2O_3	0.23	0.27	0.34	0.21	0.21	0.22	0.28	0.22
MnO	0.00	0.00	0.02	0.00	0.00	0.01	0.00	0.00
MgO	0.00	0.00	0.00	0.00	0.00	0.00	0.00	0.00
CaO	1.14	1.38	0.33	0.94	0.49	0.36	0.47	0.41
BaO	0.85	0.66	0.08	0.78	0.08	0.12	0.09	0.17
Na_2O	5.78	6.67	3.79	6.06	4.84	4.18	4.82	4.43
K_2O	6.66	5.28	10.75	6.76	8.91	9.85	9.20	9.64
Total	98.68	98.10	97.85	98.91	97.29	98.63	98.23	97.90
Formula based on O = 8								
Si	2.92	2.90	2.96	2.93	2.96	2.98	2.96	2.96
Ti	0.00	0.00	0.00	0.00	0.00	0.00	0.00	0.00
Al	1.08	1.09	1.03	1.07	1.04	1.02	1.04	1.04
Cr	0.00	0.00	0.00	0.00	0.00	0.00	0.00	0.00
Fe3	0.01	0.01	0.01	0.01	0.01	0.01	0.01	0.01
Fe2	0.00	0.00	0.00	0.00	0.00	0.00	0.00	0.00
Mn	0.00	0.00	0.00	0.00	0.00	0.00	0.00	0.00
Mg	0.00	0.00	0.00	0.00	0.00	0.00	0.00	0.00
Ca	0.06	0.07	0.02	0.05	0.02	0.02	0.02	0.02
Ba	0.02	0.01	0.00	0.01	0.00	0.00	0.00	0.00
Na	0.51	0.59	0.34	0.54	0.44	0.37	0.43	0.40
K	0.39	0.31	0.64	0.39	0.53	0.58	0.54	0.57
Cation sum	4.98	4.99	5.00	4.99	5.00	4.98	5.00	5.00
End member proportions								
An	5.82	6.98	1.65	4.71	2.45	1.81	2.35	2.06
Ab	53.55	61.16	34.31	54.94	44.10	38.46	43.28	40.28
Or	40.63	31.86	64.05	40.36	53.46	59.73	54.38	57.66

Viev) and CL spectrometer (ASK SEM-CL). The system operated in a high-vacuum mode, at 20 kV accelerating voltage, and 50 μA current. The intensity of CL spectra were normalized to 100% in terms of the intensity units.

3.5. Major and trace element analyses of whole rock

The whole-rock analyses were conducted at Bureau Veritas Minerals Laboratories Ltd. in Vancouver Canada, using LF200 package. The material of 5 g per each sample was crushed in an agate mortar and sieved before analysis. Samples prepared in this manner were then mixed with $LiBO_2/Li_2B4O_7$ flux. Crucibles were fused in a furnace. The cooled bead was dissolved in ACS grade nitric acid and analysed by combined ICP-OES (Inductively Coupled Plasma - Optical Emission Spectrometry) and ICP-MS (Inductively Coupled Plasma - Mass Spectrometry). Major and trace elements were determined using Spectro Ciros Vision and ELAN 9000 devices, respectively. Loss on ignition (LOI) was measured by igniting a sample split then measuring the weight loss. The results of whole-rock analysis for samples collected from lower, middle, and top portions of the magmatic body are presented in Table 4.

4. Results

4.1. Field description

The rocks are characterised by aphyric, fine-crystalline textures, and non-foliated, locally vesicular appearance. They reveal slight variation in terms of the colours and presence of secondary phases. The samples from the old quarry are mainly light-brown or dark-brown and contain euhedral to subhedral barite and calcite crystal of ca. 4 mm in length. They are also characterised by the presence of hard, siliceous, jasper-like rocks, which strongly contrast with magmatic rocks and form small lenses or veins in them (Fig. 2A). These jasper-like rocks exhibit greenish to brownish-red colours, sometimes with zonation, and locally reveal poorly-developed banded textures. Some of them are covered by manganese oxides forming characteristic dendritic patterns. Samples from the 2nd exp. level (new quarry) are dark-grey or dark-brown and contain light-brown or reddish-brown microcrystalline siderite aggregates. Finally, samples from the 3rd and 4th exp. levels of a new quarry exhibit greenish-brown to reddish colours.

4.2. Microscopic description

The samples reveal inequigranular (fine to medium-crystalline), holocrystalline, and locally interstitial textures. The rock matrix of the samples consists predominantly of hypautomorphic, lath-shaped, and lamellar-twinned plagioclase crystals whose lengths do not exceed 0.4 mm. Some of them exhibit an oscillatory zoning. Alkali-feldspars up to ca. 0.2 mm in size were also observed between plagioclases. Both plagioclases and alkali-feldspars are generally well preserved, except for those in the samples from the 4th exp. level (new quarry) since they are locally impregnated with dust-like speckles probably connected with weathering processes (kaolinitization, sericitization). The mafic minerals of the samples, i.e. olivine and clinopyroxene, were almost completely pseudomorphosed with uralite, chlorite, and calcite (Fig. 2B and C). Nevertheless, some fresh clinpoyroxene (augite) crystals ranging ca 0.2 mm in size could be observed in the samples from the old quarry (Fig. 2C). The volcanites contain variable amounts of

Table 3
Representative electron microprobe analyses of weakly luminescent and dark-brown luminescent albites.

Location	Old quarry		New quarry (4th exp. level)			
CL colours	Non-luminescent		Dark-brown			
Special features	Developed as elongated patches within the host plagioclase		Occurs as almost complete replacement of the host plagioclase			
wt%						
SiO_2	67.01	65.78	66.43	66.26	65.87	66.50
TiO_2	0.00	0.00	0.00	0.00	0.01	0.00
Al_2O_3	19.84	20.31	19.53	19.57	19.59	19.54
Fe_2O_3	0.04	0.10	0.01	0.19	0.18	0.08
MnO	0.00	0.01	0.08	0.01	0.00	0.00
MgO	0.00	0.00	0.00	0.00	0.00	0.00
CaO	0.03	0.29	0.05	0.04	0.08	0.04
BaO	0.00	0.00	0.02	0.01	0.00	0.00
Na_2O	11.26	11.20	11.32	11.39	11.38	11.55
K_2O	0.06	0.06	0.05	0.03	0.06	0.01
Total	98.24	97.74	97.47	97.50	97.16	97.73
Formula based on O = 8						
Si	2.98	2.94	2.98	2.97	2.97	2.97
Ti	0.00	0.00	0.00	0.00	0.00	0.00
Al	1.04	1.07	1.03	1.03	1.04	1.03
Cr	0.00	0.00	0.00	0.00	0.00	0.00
Fe3	0.00	0.00	0.00	0.01	0.01	0.00
Fe2	0.00	0.00	0.00	0.00	0.00	0.00
Mn	0.00	0.00	0.00	0.00	0.00	0.00
Mg	0.00	0.00	0.00	0.00	0.00	0.00
Ca	0.00	0.01	0.00	0.00	0.00	0.00
Ba	0.00	0.00	0.00	0.00	0.00	0.00
Na	0.97	0.97	0.98	0.99	0.99	1.00
K	0.00	0.00	0.00	0.00	0.00	0.00
Cation sum	4.99	5.01	5.00	5.00	5.01	5.01
End member proportions						
An	0.16	1.42	0.22	0.17	0.37	0.21
Ab	99.47	98.25	99.51	99.67	99.27	99.72
Or	0.37	0.32	0.27	0.16	0.36	0.07

opaque minerals, mainly magnetite. Secondary iron oxides/hydroxides (possibly hematite) mostly disseminated through the margins of olivine relics as well as apatite are also present. All samples are enriched in hydrothermal secondary phases such as carbonates, quartz, and chlorites. The carbonates and quartz usually fill the interstitial spaces between plagioclases, alkali-feldspars, and/or mafic minerals. Carbonates and chlorite form veins cutting across the groundmass of the rocks (Fig. 2D).

Jasper-like veins and lenses occurring within volcanic rocks from the old quarry are mainly built of microcrystalline quartz (<20 μm in size) with minor amounts of carbonates and micas (muscovite). The latter exhibit a well-preserved laminated (relict) texture (Fig. 2E). Furthermore, green-coloured clay-group minerals (celadonite and/or chlorite) were recognized within the silica matrix of the jasper-like rocks. They occur mainly as micaeous minute pigment or form dull clay masses. Celadonite/chlorite, associated with carbonates and other alteration products, was also frequently observed in volcanites containing jasper-like veins (Fig. 2F). The contact zone between jasper-like rocks and magmatic rocks is characterised by the presence of fibrous or spherical-shaped chalcedony aggregates.

4.3. Scanning electron microscope equipped with energy dispersive spectroscopy (SEM-EDS)

According to SEM-EDS observations (Fig. 3A-F), all of the investigated samples are characterised by the presence of primary andesine-labradorite laths surrounded by alkali-feldspars and quartz. The andesine-labradorite laths contain variable amounts of secondary albite patches disseminated through the host crystals (Fig. 3A). These patches are well-developed in the samples from the old quarry where their thickness locally exceeds 0.05 mm. The replacive albite is predominately found along polysynthetic twinning planes of the host andesine-labradorite and/or intergranular boundaries. The interface between the aforementioned mineral phases is sharp and exhibits no chemical zoning. Well-developed albitic patches are also observed in the samples from the 4th exploitation level where igneous plagioclases were almost completely converted into secondary albite (Fig. 3B-3C). SEM-BSE imaging revealed that replacive albite is noticeably porous compared with alkali-feldspars and unaltered andesines/labradorites. Kaolinite, Mg—Fe chlorites, and calcite, representing the major secondary phases associated with albitized plagioclases, fill micro-cracks and/or interstitial space between primary minerals. Additionally, numerous minute crystals of secondary Fe oxides/hydroxides are concentrated along fracture zones and cracks within the rock matrix.

The ore minerals are mainly represented by Fe-oxides/hydroxides, Ti-rich magnetite, and ilmenite. The latter tends to form fine (up to 5 μm) trellis-type or minor larger sandwich-type exsolution lamellas. According to e.g. Buddington and Lindsley (1964) and Haggerty (1991), trellis type intergrowths are composed of ilmenite lamellae located along the {111} planes of the titanomagnetite host while sandwich type is described as a small number of ilmenite laths along one set of the octahedral planes of the titanomagnetite - Fig. 3D and E. These intergrowths are often highly porous. Locally, granules or laths of ilmenite occur on the margins of Ti-magnetite, whereas densely-packed ilmenite was also observed at the contact with fluoroapatite (Fig. 3D).

Fluoroapatite appears fairly homogenous in BSE images and occurs as acicular hypidiomorphic to idimorphic crystals, which are sometimes ragged or fractured and locally contain small Ti-magnetite inclusions. Moreover, fluoroapatite is the most abundant in the samples from the 4th exp. level (new quarry) and seems to be closely associated with magnetite crystals, as well as alteration products of the mafic minerals. SEM-EDS observations confirmed the presence of celadonite in the samples containing jasper-like veins (Fig. 3E). The minute hypidiomorphic zircon crystals forming inclusions within chlorite were also identified during BSE observations (Fig. 3F).

4.4. Electron microprobe analysis (EMPA) and WDXS elemental maps

EMP analyses coupled with WDXS elemental mapping revealed systematic variations of chemical composition within species of plagioclases (Table 1) and alkali-feldspars

(Table 2). The lath-shaped plagioclase crystals have composition of $An_{39\text{-}50}Ab_{47\text{-}58}Or_{23}$. The alkali-feldspars filling the interstitial space between plagioclases form 2 zones of slightly different proportions of Na and K (Fig. 4). An Ab-rich zone (ca. 0.1 mm thickness) with Na/K mol. ratio up to 1.9 occurs in the closest vicinity of andesine-labradorite crystals and is further followed by an Or-rich zone (Na/K mol. ratio up to 0.83) that, in turn, sharply contrasts with the interstitial quartz. The former zone is characterised by an end member composition of $An_{2\text{-}7}Ab_{34\text{-}61}Or_{32\text{–}64}$ and contains a relatively high amounts of TiO_2 (up to 0.09 wt. %) and BaO (up to 0.85wt.%). Additionally, it reveals the presence of discrete strings made of nearly pure albite, which are situated perpendicular to the grain boundary of the plagioclase host and slightly resemble perthitic textures. In contrast, the Or-rich zone has an end member composition of $An_2Ab_{38\text{-}44}Or_{54\text{–}60}$ while its TiO_2 and BaO contents do not exceed 0.04 and 0.17 wt.%, respectively. The replacive albite forming patches within host andesine or labradorite has nearly end member composition with an Ab content up to 99.72 mol.% (Table 3).

4.5. Cathodoluminescence microscopy (OM-CL) and spectroscopy

The cathodoluminescence observations revealed that plagioclases and alkali-feldspars exhibit variable luminescence colours (Fig. 5A-F). The lath-shaped plagioclases (andesine-labradorite) luminescence mostly greenish to greenish-grey, which is related to a relatively low An content. The green luminescence of plagioclases indicates Ca^{2+} -

Table 4
Whole-rock major and trace element composition of trachyandesites from Świerki quarry.

Location	Old quarry		New quarry					
			2nd exp. level		3rd exp. level		4th exp. level	
Sample	MD-SP1	MD-SP2	MD-SP3	MD-SP4	MD-SP5	MD-SP6	MD-SP7	MD-SP8
Major element (wt%)								
SiO_2	56.38	56.27	55.99	55.72	55.36	55.05	55.37	55.48
TiO_2	1.45	1.45	1.39	1.37	1.42	1.42	1.42	1.42
Al_2O_3	15.81	15.87	15.20	15.27	15.58	15.68	15.70	15.52
FeO_t	7.94	7.89	8.69	8.67	7.37	7.39	8.90	8.84
MnO	0.12	0.12	0.12	0.13	0.16	0.16	0.05	0.04
MgO	2.71	2.72	2.34	2.37	1.36	1.36	4.43	4.40
CaO	4.86	4.90	5.56	5.59	7.40	7.32	2.25	2.22
Na_2O	4.16	4.16	3.52	3.50	3.42	3.40	3.13	3.13
K_2O	2.97	2.99	2.86	2.86	2.60	2.64	2.39	2.35
P_2O_5	0.57	0.58	0.55	0.54	0.57	0.57	0.58	0.58
L.O.I.	2.70	2.70	3.40	3.60	4.40	4.70	5.50	5.70
Total	99.67	99.65	99.62	99.62	99.64	99.69	99.72	99.68
Mg#	0.38	0.38	0.32	0.33	0.25	0.25	0.47	0.47
$Na_2O + K_2O$	7.13	7.15	6.38	6.36	6.02	6.04	5.52	5.48
CaO/Na_2O	1.17	1.18	1.58	1.60	2.16	2.15	0.72	0.71
Trace element (ppm)								
Be	<D.L.	2.00	3.00	3.00	< D.L.	2.00	4.00	5.00
Sc	17.00	17.00	16.00	16.00	17.00	17.00	17.00	17.00
V	113.00	114.00	108.00	109.00	112.00	112.00	107.00	111.00
Cr	17.10	17.10	20.52	13.68	20.52	17.10	17.10	17.10
Co	20.10	19.40	19.40	18.50	18.30	18.50	29.30	31.40
Ni	22.00	< D.L.	< D.L.	< D.L.	22.00	20.00	23.00	23.00
Ga	21.20	21.50	20.40	19.90	21.60	21.10	21.90	22.80
Rb	83.30	83.30	73.80	72.50	69.70	70.00	65.80	64.40
Sr	327.10	324.00	304.80	296.70	278.10	276.50	62.40	60.30
Cs	0.90	1.30	0.70	0.40	0.80	0.90	2.80	2.90
Y	50.80	49.70	45.90	44.50	43.20	44.90	42.60	40.70
Zr	543.70	544.00	506.00	501.10	548.70	549.90	531.50	529.00
Nb	36.20	36.50	34.70	34.60	35.50	36.20	36.40	36.70
Ba	668.00	655.00	939.00	910.00	855.00	877.00	529.00	537.00
Hf	10.70	11.10	11.10	11.20	12.00	11.80	11.90	11.60
Ta	2.00	2.10	2.00	2.00	1.90	1.90	2.20	2.10
Th	10.50	10.80	11.40	11.00	10.90	10.30	10.90	10.70
U	4.80	4.30	3.50	3.10	3.00	3.20	2.80	2.50
La	81.90	82.70	81.00	79.10	79.70	79.20	78.50	78.80
Ce	161.50	159.90	157.00	153.80	152.90	158.10	156.80	157.80
Pr	18.01	17.66	17.49	17.15	16.99	17.22	17.36	17.43
Nd	67.10	65.60	66.60	63.40	64.20	65.30	66.30	65.60
Sm	12.35	12.15	11.70	11.65	11.42	11.58	11.21	11.65
Eu	2.83	2.66	2.48	2.39	2.50	2.56	2.19	2.19
Gd	11.63	11.11	10.76	10.25	10.22	10.60	9.87	10.11
Tb	1.72	1.66	1.57	1.54	1.55	1.55	1.47	1.40
Dy	9.47	9.49	8.82	8.56	8.44	8.62	7.79	8.09
Ho	1.89	1.84	1.77	1.73	1.69	1.67	1.63	1.59
Er	5.42	5.28	4.93	4.96	4.93	4.80	4.69	4.70
Tm	0.77	0.72	0.71	0.73	0.70	0.69	0.69	0.66
Yb	4.68	4.71	4.46	4.62	4.30	4.40	4.55	4.33
Lu	0.70	0.70	0.69	0.67	0.68	0.66	0.67	0.66
REE sum	379.97	376.18	369.98	360.55	360.22	366.95	363.72	365.01
LREE/HREE	14.41	14.42	15.12	14.81	15.16	15.39	15.93	16.03
$[La/Yb]_{CN}$	11.89	11.93	12.34	11.63	12.59	12.23	11.72	12.36
$[La/Sm]_{CN}$	4.14	4.25	4.32	4.24	4.36	4.27	4.37	4.22
$[Gd/Yb]_{CN}$	2.01	1.91	1.95	1.79	1.92	1.95	1.76	1.89
$[Nb/Th]_{PM}$	0.42	0.41	0.37	0.38	0.39	0.42	0.40	0.41
$[Ta/Th]_{PM}$	0.41	0.42	0.38	0.39	0.37	0.40	0.43	0.42
Eu/Eu^*	0.73	0.70	0.68	0.66	0.70	0.71	0.63	0.63

Note: FeO_t - total Fe as Fe^{3+}; L.O.I. - loss on ignition; D.L. - detection limit; Mg# - molar Mg/(Mg + Fe).
$Eu^* = (Sm_{CN} \cdot Sm_{CN} \cdot Tb_{CN})^{1/3}$ -see: Lawrence et al. (2006); $_{CN}$ - chondrite-normalized; $_{PM}$ - primitive-mantle normalized.

Mn^{2+}-substitution that acts as a primary CL activator (e.g. Mora and Ramseyer, 1992). Ab-rich alkali-feldspars appearing in the near vicinity of the boundary with host andesines-labradorites exhibit bright-blue luminescence colours, whereas Or-rich alkali-feldspars are characterised by dull-blue CL (Fig. 5A-B). Interstitial quartz is weakly-luminescent, although some crystals are marked by distinctive red-dish-brown to dark-brown luminescence associated to lattice defects produced by twinning, mechanical deformation, or rapid growth (Ramseyer et al., 1988). The boundaries between different luminescing zones of andesines-labradorites and alkali-feldspars are sharp and locally frayed since no gradual zonation is observed, while the contact zones between quartz and Or-rich alkali-feldspars revealed numerous embayments (Fig. 5B and F). Albite patches found within primary plagioclases exhibit a lack of luminescence colours (Fig. 5C). On the other hand, almost completely albitized plagioclases from top portions of the magmatic body in the new Świerki quarry revealed a change of

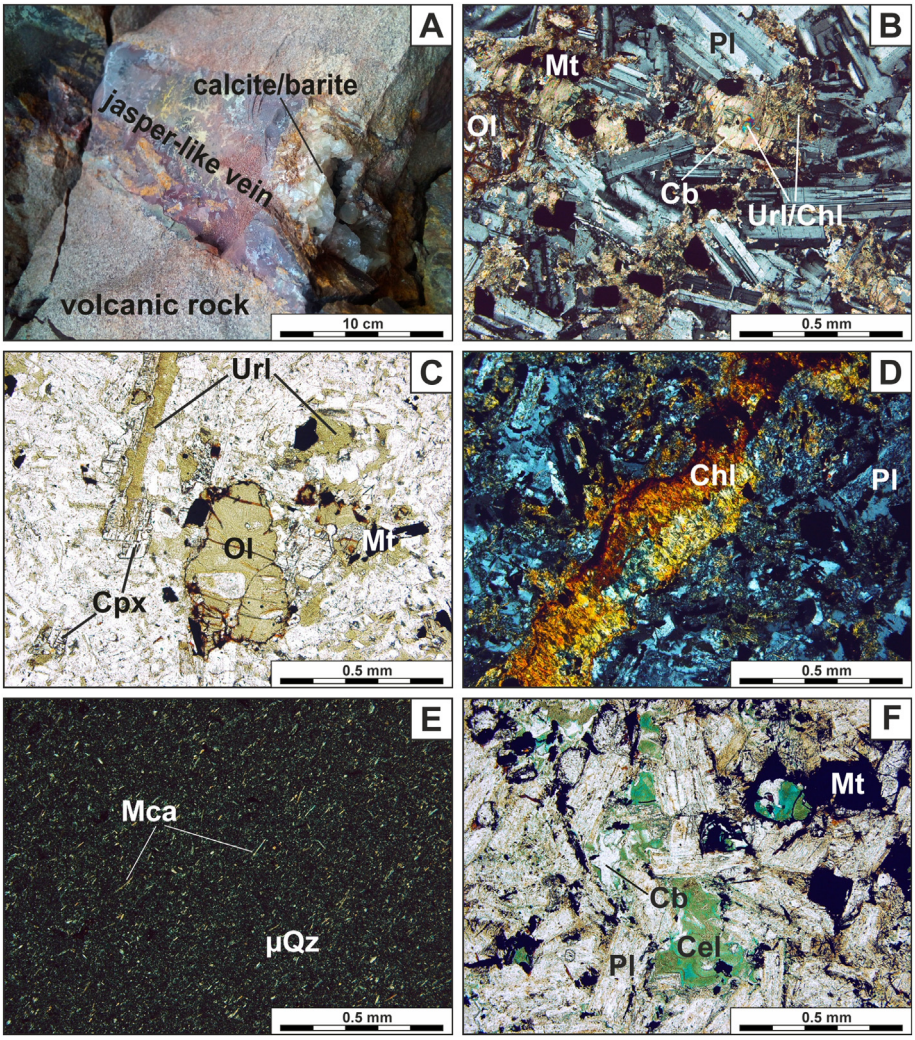

Fig. 2. Photographs (A) and photomicrographs (B—F) of volcanic rocks from Świerki quarry. (A) Jasper-like vein associated with calcite/barite crystals and surrounded by light-brown trachyandesite (old quarry); (B) Trachyandesite from the new quarry (2nd exp. level) containing igneous plagioclases (Pl), magnetite (Mt) and mafic minerals including pyroxene (Px) and olivine (Ol) - the latter were completely replaced with uralite/chlorite (Url/Chl) and carbonates (Cb); (C) Oriented replacement of clinopyroxene (Cpx) with uralite (Url) characterised by the presence of uralite fibres situated parallel to {001} planes of pyroxene; (D) Chlorite (Chl) vein from the spilitic rocks of 4th exp. lvl. (new quarry); (E) Jasper-like vein consisting of microquartz (μQz), mica group minerals (Mca), and exhibiting well-preserved laminated texture; (F) Celadonite (Cel) followed by carbonates (Cb) from the contact zone between magmatic rock and jasper-like vein.

greenish CL colours into brownish (5D-5F). Fine carbonate particles disseminated through the rock matrix exhibit mostly orange-yellow luminescence connected with the substitution of Ca^{2+} by Mn^{2+} (e.g. Habermann et al., 2000). Locally, carbonates are characterised by vanishing of CL colours that may indicate the presence of siderite and/or ankerite since Fe is the main quencher in this group of minerals (Machel et al., 1991). Fluoroapatite crystals exhibit predominantly homogenous violet/pink and subordinately yellowish CL colours. The yellow CL colours of fluoroapatite was frequently observed in small grains closely related to alteration zones (chloritization, carbonatization, etc.), whereas violet/pink luminescence is dominant among larger crystals dispersed within the rock matrix. Some of the violet/pink luminescent fluoroapatites reveal a distinctive zonation since they contain yellowish overgrowths developed along the rims and fracture zones of the crystals.

The CL spectra of 3 generations of feldspar-group minerals, exhibiting greenish-grey, light-blue, and dark-blue CL are presented in the Fig. 6A, B, and C. All spectra consist of a broad blue band centred between 450 and 480 nm, which is related to either Al-O^--Al centres or Al-O-Ti bridges. The peak located at around 700 nm is associated with the structural state of the feldspars and/or the occupancy of the Al^{3+} tetrahedral site by Fe^{3+} (e.g. Götze, 2012; White et al., 1986). The red peak of alkali-feldspars shifts from 704 nm in Ab-rich alkali-feldspars (Fig. 6B) to 689 nm in Or-rich alkali-feldspars (Fig. 6C). This is probably due to K—Na substitution in their structure. The presence of the larger potassium ion in the feldspar structure causes stretching of the crystal lattice, variation of the cell dimensions and downshift of the characteristic peaks in the CL spectrum (Kayama et al., 2010; Krbetschek et al., 2002). Moreover, the intensity of the Al-O^--Al/ Al-O^--Ti-related emission line prevails over the Fe^{3+}-induced band (I_B/I_R ratios vary from ca. 2 in Ca-rich plagioclase and K-feldspar to ca. 5 in Na-feldspar).

The spectrum of violet-pink luminescent fluoroapatite contains strong emission lines located in the range of 380–470 nm which are characterised by nearly equal intensity and should be ascribed to the presence of REE^{3+}-activators including Ce^{3+} (379 and 398 nm), Tb^{3+} (435 nm), and Dy^{3+} (470 nm) - see Fig. 6D. Additionally, the spectrum consists of a broad band with maximum at 576 nm and related to Ca^{2+}-Mn^{2+} substitution in apatite structure (Götze, 2012; Kempe and Götze, 2002). The CL spectrum of yellow luminescent apatite is generally similar to that collected from violet-pink luminescent crystals, as it contains a dominant Ce^{3+}-activated band located at 380 nm (Fig. 6E). However, the intensity of the Ce^{3+} emission line is dominant as it significantly prevails over bands activated by Tb^{3+} (433 nm) and Dy^{3+} (470 nm).

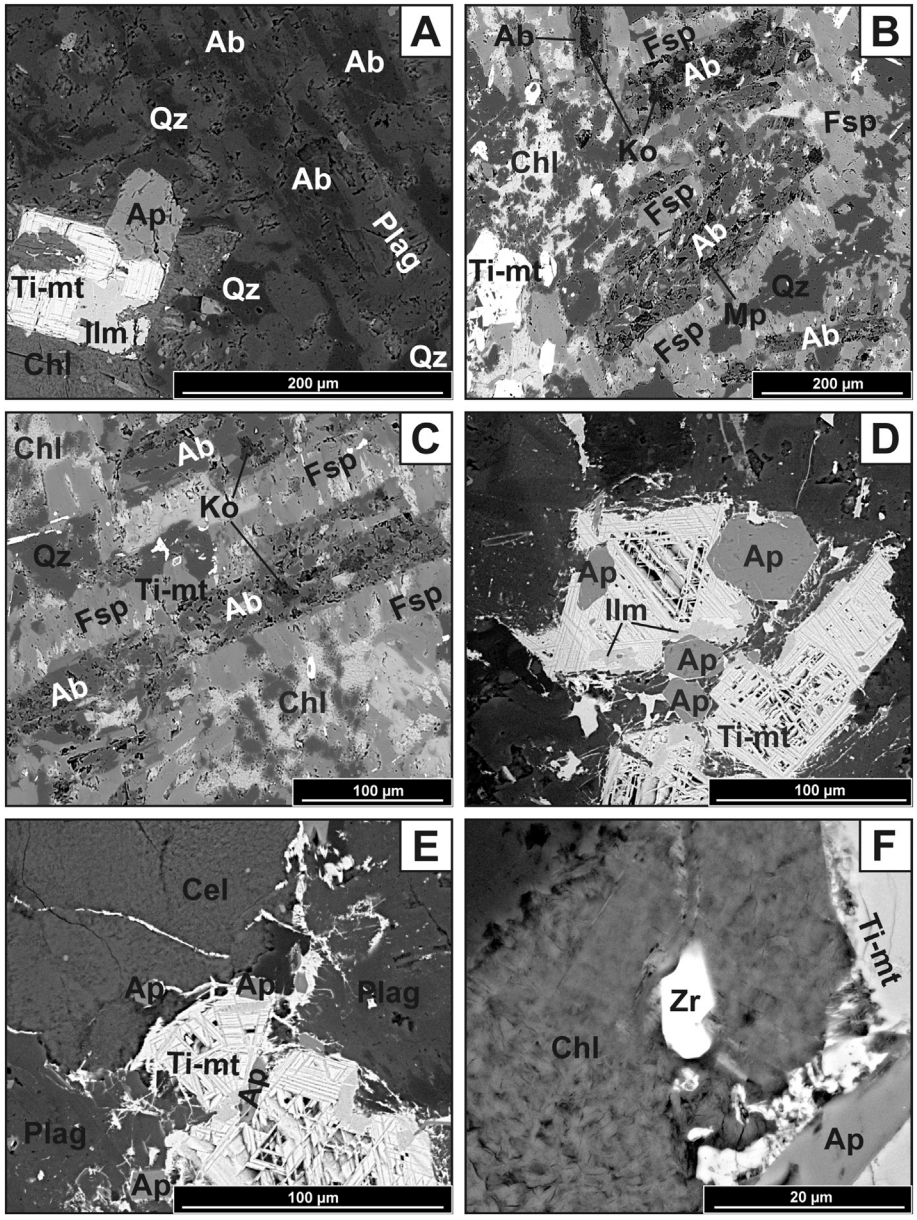

Fig. 3. BSE images of volcanites from the old quarry. (A,B) Albitized plagioclase (Ab) accompanied by kaolinite (Ko) and Fe—Mg chlorite (Chl). The close association between replacive albite and micropores (Mp) should be noted. (C) Secondary albite patches (Ab) developed along polysynthetic twinning planes of the primary andesine (Plag); (D) Ti-rich magnetite (TiMt) containing thin trellis-type ilmenite (Ilm) intergrowths surrounded by numerous fluoroapatite (Ap) crystals; (E) Celadonite pigment (Cel) at the contact with titanomagnetite (TiMt); (F) Zircon (Zr) embedded in chlorite-group minerals (Chl).

4.6. Bulk-rock chemistry

The rocks are characterised by similar SiO_2 concentrations varying between 55.05 and 56.38 wt% (Table 4). The contents of Al_2O_3 (~15.58 wt%), FeO_t (~8.21 wt%) together with TiO_2 (~1.42 wt%), Cr_2O_3 (~0.005 wt%), P_2O_5 (~0.57 wt%) do not present significant variations among the samples as well. Otherwise, variable amounts of CaO ranging from 2.24 to 7.36 wt.% were noted. Furthermore, CaO correlates negatively with both MgO ($r = -0.99$) and Fe ($r = -0.79$) and positively with MnO ($r = 0.98$). Mg# values (the molar ratio of Mg/(Mg + Fe)) are relatively low and range from 0.25 to 0.47. The samples are remarkably enriched in alkalis ($Na_2O + K_2O$), whose content exceeds 6.0 wt.%. All of them exhibit the predominance of Na_2O over K_2O. CaO/Na_2O ratios vary from 0.71 to 2.16 and generally meet the standards for spilites ($CaO/Na_2O < 1.9$, see Fu and Wang, 1984). The normative composition of the rocks, calculated using the CIPW method, revealed the presence of such mineral components as: quartz, plagioclase, diposide, hypersthene, apatite. The anorthite content in normative plagioclase is variable and ranges from about 15% (samples from the 4th exp. level) to almost 40% (samples from the 3rd exp. level). Finally, LOI values occur in a wide range (2.7–5.7 wt.%) and are not remarkably correlated with TiO_2, P_2O_5, or Cr_2O_3 contents. The Rb/Sr ratio, which increases with the alteration degree and reflects the effects of secondary alteration on LILE redistribution (Lefleche et al., 1992), varies from ca. 0.25 (samples from old quarry and lower levels of a new quarry) to ca. 1.06 in rocks collected from the upper parts of the magmatic bodies. Following the classification of the rocks based on inter-element relationships between Zr/TiO_2–Nb/Y and Zr/TiO_2–Ga (Winchester and Floyd, 1977), the investigated rocks belong to either the trachyandesite or the rhyodacite series, respectively.

The total REE concentrations are generally high and range from 360 to 380 ppm. Chondrite-normalized REE patterns are sub-parallel and rightward-inclined (Fig. 7A). They exhibit minor europium anomalies (Eu/Eu^*) within the range of 0.63–0.73. The patterns are characterised

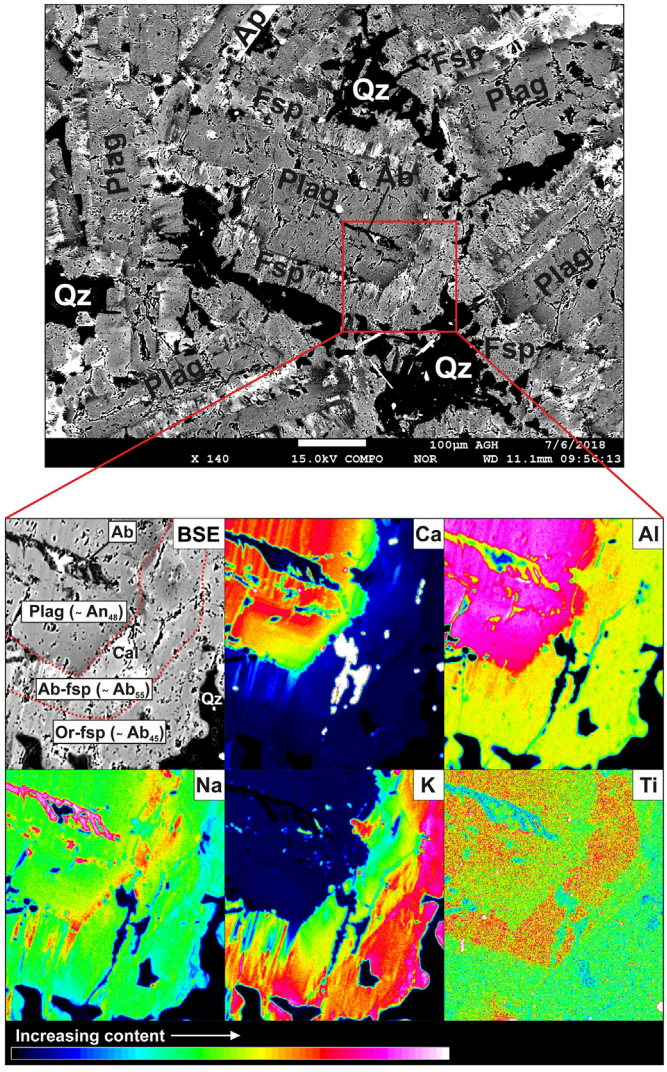

Fig. 4. BSE image of volcanic rocks from the 3rd exploitation level coupled with WDXS elemental maps of Ca, Al, Na, K, and Ti revealing compositional variations within feldspar-group minerals. It should be noted that the area enriched in alkali-feldspars (outwards from the plagioclase margin) is divided into Ab-rich zone (Ab~55%) followed by Or-rich zone (Ab~45%), while minor albite patches (Ab~99%) penetrate through andesine crystals. Abbreviations: Plag - plagioclase (andesine); Fsp - alkali-feldspars; Ab - secondary albite; Cal - calcite; Ap - fluoroapatite; Qz - quartz.

by gentle slopes for the LREE (La_{CN}/Sm_{CN} ratios vary from 4.14 to 4.37) and plateaus for the HREE (Gd_{CN}/Yb_{CN} ratios vary from 1.76 to 2.01). Additionally, the curves reveal high LREE-enrichments relative to HREE since La_{CN}/Yb_{CN} ratios range from 11.63 to 12.59. The shape of REE patterns resembles those reported from continental tholeiites exhibiting $[La/Yb]_{CN}$ values up to 12 (Dupuy and Dostal, 1984). Trachyandesites are simultaneously far more LREE-fractionated relative to spilite-keratophyre association from the Western Sudetes (Narebski et al., 1986).

Primitive-mantle normalized multi-elements patterns of the samples have also a similar shape (Fig. 7B). They are characterised by enrichment in some large ion lithophile elements (LILE) such as Ba, Rb, and K, whereas Sr reveals distinctive negative anomalies. The samples exhibit positive spikes for high field strength elements (HFSE) including Zr, Hf, U, and Th. On the contrary, significant depletion of Nb, Ta, P, and Ti is marked on the patterns. The multi-element pattern for rocks from the 4th exp. level reveals simultaneously a relatively higher negative Sr anomalies and a relative increase of the Cs content as opposed to the rest of the samples.

5. Discussion

5.1. The evolution of mineralogical composition of the rocks

Our complex CL, SEM-EDS, and SEM-EMPA study were used to revise the data published by Dziedzicowa (1958), who based mostly on polarizing microscopy during her investigations on trachyandesites from Świerki quarry. According to this author, albitization of plagioclase is a ubiquitous feature of these rocks and occurred during a late stage of magma differentiation due to auto-hydrothermal processes. The alteration resulted in the presence of pure albite rims surrounding primary plagioclases and was then post-dated by crystallization of K-feldspar and quartz (Dziedzicowa, 1958). Although the presence of secondary albite was confirmed in this study, we excluded its formation in the external parts of primary plagioclases (andesine-labradorite). Instead of that, andesines and labradorites from the investigated samples are rimmed by two generations of alkali-feldspars: (1) bright-blue luminescent Ab-rich and (2) dull-blue luminescent Or-rich one (Fig. 8). The acquired data does not provide clear textural evidence (lack of secondary porosity or pseudomorphic character) that those alkali-feldspars formed directly due to Na-induced metasomatism since they luminescence in a manner typical of magmatic (high-temperature) feldspars (e.g. Kastner, 1971; Kayama et al., 2010). Hence, both bright-blue and dull-blue luminescent alkali-feldspars occupying space between primary plagioclases have possibly crystallized directly from the melt during later stages of rock evolution (see: Brown, 1993) and remained intact during albitization processes. The high TiO_2 content of the bright-blue luminescent alkali-feldspars relative to the dull-blue ones further suggest that the former crystallized at higher temperatures (see: Götze et al., 2000; Smith and Brown, 1988), which is consistent with crystallization from a cooling melt. The elevated BaO concentration in blue luminescent areas might have been favoured by decreasing pressure and temperature, as well as high activity of fluids during rock formation (Guo and Green, 1989).

Mineralogical and textural features point to intensive alteration of the volcanites from Świerki quarry, which is consistent with previous studies concerning these rocks (Dziedzicowa, 1958; Nowakowski, 1968). Their final mineral composition was determined by the melt differentiation and later on, as a result of hydrothermal-metasomatic reactions during post-magmatic stage. Albitization of plagioclases (andesine-labradorite) is a common feature of the rocks and seems to be closely associated with carbonatization and chloritization. The highest alteration degree was observed in the samples collected from the old quarry and the top portions of the new quarry where plagioclases (andesine-labradorite) were partially or almost completely converted into albite. The secondary (replacive) albite is developed within internal part of host andesines or labradorites and forms elongated patches along polysynthetic twinning planes and/or intergranular boundaries. According to EMP analysis and CL observations, these patches exhibit nearly end member composition (most of them have Ab>99 mol.%) and are characterised by weakly-luminescent to brown-luminescent character (Fig. 8). The above features are consistent with those reported for authigenic (secondary) albites from sedimentary and low-grade metamorphic rocks (Fedo et al., 1997; González-Acebrón et al., 2012; Kastner, 1971; Richter et al., 2002). The lack of luminescence in secondary albite reflects its chemical purity and may be ascribed to the ordering of the crystal lattice and/or healing of structural defects due to fluid-feldspar interactions (e.g. Fedo et al., 1997; Finch and Klein, 1999; Kayama et al., 2010), while brown luminescence colours argue for depletion in Na or a structural defect in the SiO_4-tetrahedron level (Wendler et al., 2012). These observations point to the presence of low-temperature albitization in altered volcanites, which occurred as a result of the high activity of alkaline-bearing hydrothermal fluids during the post-magmatic stage of the rocks' formation. The sharp chemical interface between albite and host plagioclase (andesine-labradorite), as well as the development of secondary

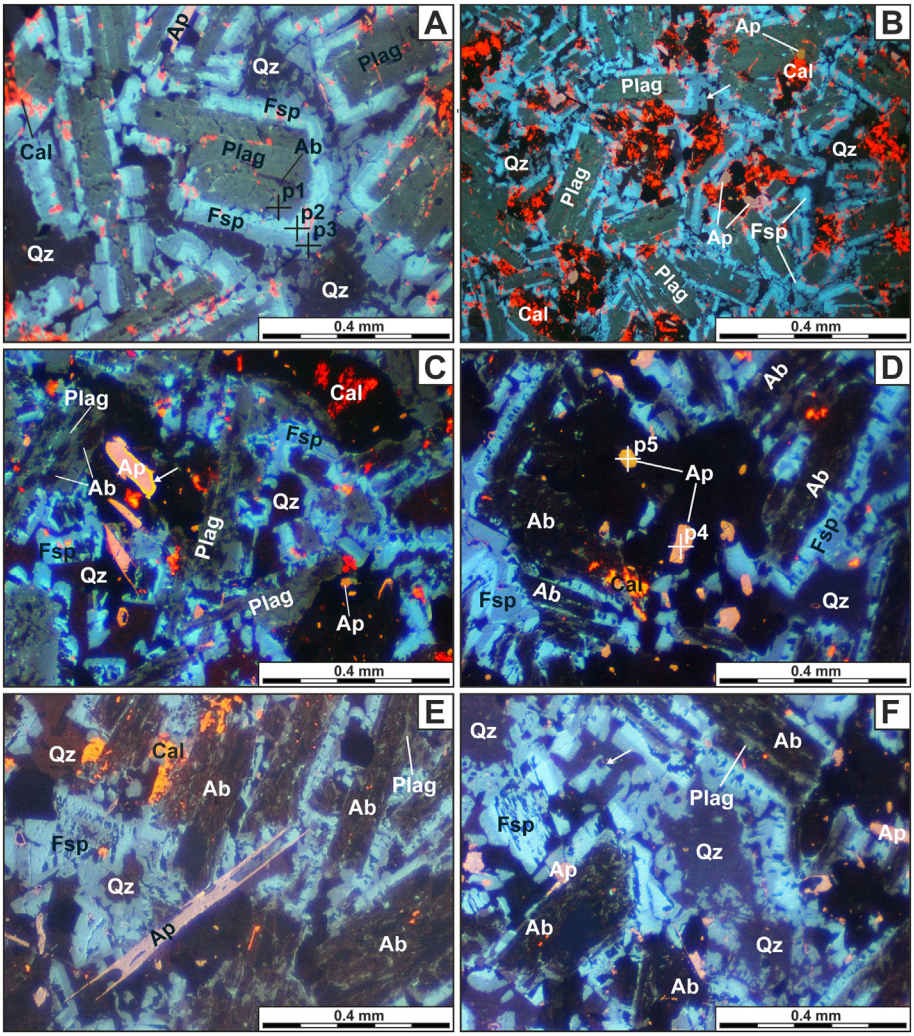

Fig. 5. CL images of volcanites from Świerki quarry; (A-B) Lath-shaped andesines (greenish-grey CL) surrounded by successive Ab-rich (bright-blue CL) and Or-rich (dull-blue CL) layers made of alkali-feldspars (sample from the 2nd exp. level) accompanied by calcite; white arrow points to embayment of alkali-feldspars at the contact with quartz; (C) Andesine laths containing weakly luminescent patches of replacive albite (sample from old quarry); white arrow points to yellowish glow developed on pink luminescent fluoroapatite; (D-E) Pervasive replacement of andesine (greenish-grey CL) by dark-brown luminescent albite; 2 generations of fluoroapatite, displaying violet-pink and yellowish CL, as well as reddish-brown quartz are also observed (samples from the 4th exp. level); (F) Embayment of blue luminescent alkali-feldspars at the contact with quartz; alkali-feldspars also occur as remnant islands, which are embedded in quartz and display numerous embayments (white arrow). Points for SEM—CL spectral analysis are marked as black/white crosses. Abbreviations: Plag - plagioclase (andesine); Fsp - alkali-feldspars; Ab - secondary albite; Cal - calcite; Ap - fluoroapatite; Qz - quartz.

micro-porosity, are consistent with an interface-coupled dissolution-reprecipitation process (see: Engvik et al., 2008; Hövelmann et al., 2010; Putnis, 2002) that was previously postulated to explain the albitization phenomenon in numerous magmatic or sedimentary rocks (see e.g. Kontonikas-Charos et al., 2017; Plümper and Putnis, 2009). The alkaline-bearing metasomatizing solutions could gain access to the grain interior through micro-cracks and micro-veins generated through hydraulic fracturing by fluid themselves or/and contractional cooling forces (Que and Allen, 1996). The latter resulted in the development of extensional fractures (joints) that were frequently observed in old and new Świerki quarry (Kozłowski, 1958, 1963). Regarding the fact albitization was a selective process as albite crystallized predominately along polysynthetic twinning planes of plagioclase (andesine-labradorite), the crystallographic orientation of twinning could also control fluid infiltration by providing the potential fluid channels.

The reaction leading to the formation of secondary albite in rocks from Świerki quarry may be expressed by the following equations (based on data provided by e.g. Engvik et al., 2008):

$$Na_{0.7}Ca_{0.3}\,Al_{1.3}Si_{2.7}\,O_8\ (\text{andesine}) + 0.6Na^{+}(\text{aq.}) + 1.2H_4SiO_4\ (\text{aq.}) \rightarrow 1.3NaAlSi_3O_8\ (\text{albite}) + 0.3Ca^{2+}(\text{aq.}) + 2.4H_2O^{-}\ (\text{aq}) \quad (1)$$

$$Na_{0.7}Ca_{0.3}\,Al_{1.3}Si_{2.7}\,O_8\ (\text{andesine}) + 0.3Na^{+}(\text{aq.}) + 0.3H_4SiO_4\ (\text{aq.}) \rightarrow NaAlSi_3O_8\ (\text{albite}) + 0.3Ca^{2+}(\text{aq.}) + 0.3Al^{3+}(\text{aq.}) + 1.2OH^{-}\ (\text{aq.}) \quad (2)$$

According to the first equation, all of the Al^{3+} released during alteration is being consumed by secondary albite. The lack of secondary Al-bearing minerals such as micas or epidote within albitized plagioclases from the investigated rocks implies that the aforementioned reaction seem to be more relevant for the formation of albite patches recognized in this study. The second reaction, which assumes high mobility of Al^{3+}, also cannot be totally excluded since Al^{3+} might have been removed

together with output fluids. According to Hövelmann et al. (2010. see also: Ramseyer et al., 1992), alkaline-bearing solutions are capable of mobilizing high amounts of aluminium as well as other trace elements. Moreover, the absence of other Al-bearing minerals apart from secondary albite may be related to an insufficient amount of K^+ in the albitizing fluids that is necessary for the formation of mica-type minerals. Carbonates, which represent a major secondary phase, have likely sourced Ca^{2+} from the primary plagioclase. Their presence points simultaneously to a relatively high CO_2 partial pressure that contributed to the alteration of plagioclase (Leichmann et al., 2003).

The source of Na^+ and Si^{4+} is also of vital importance while considering the albitization phenomenon. According to Dziedzicowa (1958) the origin of Na-bearing fluids was related to autometasomatic processes (excluding the external derivation of Na^+ from i.e. sea-water). CL microscopy and BSE observations revealed that alkali-feldspars exhibit numerous embayments at the contact with quartz. These observations suggest feldspars were partially dissolved during interaction with hot magma or/and high-temperature fluids and thus could become capable of providing a necessary source of Si^{4+} and Na^+.

Not only were the fluid-mineral interactions revealed by CL microscopy and SEM-EDS and EMPA analysis of feldspars, but also the luminescence behaviour of fluoroapatite reflected the fluctuations of physicochemical condition during crystallization and/or the activity of secondary fluid flows. According to Kempe and Götze (2002); see also: Słaby and Götze, 2004), violet/pink (REE^{3+}-activated) fluoroapatite, typical of carbonatites and other alkaline rocks, could possibly be formed under alkaline conditions. In contrast, a yellowish

(Mn^{2+}-activated) CL feature of apatite, which was reported from e.g. P-rich granites, reflects a relatively more acidic environment (Kempe and Götze, 2002; Mariano, 1988). Changes of physicochemical conditions of crystallization (alkaline-acidic) reported for the volcanic rocks from this study are possibly related to albitization processes, which are favoured in the presence of fluids characterised by low pH (Ramseyer et al., 1992) Additionally, the yellowish-luminescent fluoroapatite crystals could crystallize from interstitial fluids since they have relatively small grain size and tend to group within the alteration zones (see: Xing and Wang, 2017). The larger crystals, exhibiting violet/pink CL and containing magnetite inclusions, are possibly of magmatic origin and were overprinted by late-stage fluid metasomatism. Finally, the reddish-brown CL colours of quartz also might have been imposed by interaction with deuteric fluids, as reported by Betsi and Lentz (2010).

Celadonite found within rock matrix is peculiar to submarine basalts altered by seawater (e.g. Odin et al., 1988), although it was also reported from continental volcanic rocks (e.g. Baker et al., 2012). The occurrence of this mineral phase in the investigated volcanites is confined solely to the contact zone between trachyandesites and jasper-like rocks. The latter were recognized as clay xenolithes that were raised by lava and subsequently altered by silification, carbonatization, and celadonitization. Their partial dissolution due to contact with hot magma could provide the sufficient source of K^+ and other elements, which are essential for the celadonite formation. Hence, the presence of celadonite in volcanites from Świerki quarry cannot argue for the presence of water-rock interactions that may significantly contribute to the formation of spilitic rocks (e.g. Munhá and Kerrich, 1980).

5.2. Luminescence activators in alkali-feldspars

Alkali-feldspars are well-known for the occurrence of CL emission at blue wavelengths, whose exact nature remains not entirely understood. Firstly, blue luminescence colours may be ascribed to paramagnetic defects connected with the substitution of Al^{3+} by Si^{4+} ($Al\text{-}O^-$-Al centres) in the feldspar structure (Finch and Klein, 1999; Götze et al., 2000; Marfunin, 1979). The $Al\text{-}O^-$-Al centres are frequently observed in feldspars except for those of high An content (Speit and Lehmann, 1982). On the contrary, Mariano et al. (1973); see also: Lee et al., 2007; Parsons et al., 2008) suggested that blue emission band at ca. 460 nm is strongly affected by the presence of a tetrahedral Ti^{4+} activator forming Al-O-Ti bridges.

Our study reveals that there is a positive correlation between the intensity of blue luminescence colours and the TiO_2 concentration among alkali-feldspars, which occur in the interstitial space between primary plagioclases (andesine-labradorite). TiO_2 concentrations in bright-blue luminescent areas vary between 0.05 and 0.09 wt.%, while dull-blue luminescent zones contain only up to 0.04 wt.% of TiO_2. The role of a Ti^{4+} impurity as an activation centre is thus highly presumable. On the other hand, the BaO content is also positively correlated with the intensity of CL emission at blue wavelengths since it ranges from ca. 0.59 wt.% in bright-blue luminescent feldspars to ca. 0.12 wt.% in dull-luminescent ones. The incorporation of Ba^{2+} into the feldspar structure is related to a coupled $K^+ + Si^{4+} \leftrightarrow Ba^{2+} + Al^{3+}$ substitution required for a charge balance. The above-mentioned exchange causes a structural distortion and thus contributes to an increasing density of the $Al\text{-}O^-$-Al defects (Słaby et al., 2008; Viswanathan and Kielhorn, 1983). Therefore, both $Al\text{-}O^-$-Ti and $Al\text{-}O^-$-Al centres are likely involved in the blue CL emission in the case of alkali-feldspars reported for the investigated rocks.

5.3. Oxidation features

The presence of regular sandwich and/or trellis type lamellas of ilmenite, developed within the host Ti-magnetite, should be attributed to a sub-solidus intra-oxide re-equilibration process known as oxy-exsolution (Buddington and Lindsley, 1964). According to Haggerty (1991); see also: Mücke, 2003; Orlický, 2010), the microtextures of ilmenite intergrowths are strongly dependent on the degree of oxidation and diffusion as well as temperature conditions. Overall, 7 stages (C1-C7) of oxidation may be distinguished on the basis of BSE imaging and/or reflected light observations (Haggerty, 1991). Following this classification, ilmenite-titanomagnetite intergrowths in trachyandesites from Świerki belong to the C2 and C3 stages of the high-temperature oxidation and formed at temperatures above 600 °C. It should be noted that a two-oxide geothermometer, based on ilmenite-magnetite pair providing exact values of re-equilibration temperatures and oxygen fugacity, has been proposed by Andersen and Lindsley (1985). Nevertheless, its application to rocks from Świerki quarry was abandoned due to secondary alteration and the coexistence of Ti-magnetite with hematite - the latter could be a product of high-temperature oxidation (C5 stage) and/or low-temperature alteration. The presence of the exsolution patterns of ilmenite-magnetite pairs instead of non-exsolved Ti-magnetite suggests that rocks had undergone a relatively slow cooling (cf. Geuna et al., 2014), supporting the idea that they were emplaced as subvolcanic intrusions (see e.g. Birkenmajer et al., 1968).

5.4. Petrotectonic implications

The discrimination parameters involving inter-element relationships of immobile elements (Nb, Y, Ga, Sc) indicate a calc-alkaline nature of the investigated trachyandesites (Winchester and Floyd, 1977). The investigated rocks have Nb/Y ratios at the level of ca. 0.8, whereas Ga/Sc ratios are up to 1.34. Calc-alkaline affinity is also supported by the Zr + Y–TiO_2–Cr relationship (see: Davies et al., 1979) and high Zr/Y ratios exceeding the value of 7.0 (MacLean and Barrett, 1993). Assuming the fact that composition of low-grade metamorphic rocks may be strongly affected by secondary alteration processes, the tectonic discrimination was solely based on the concentration of such trace elements, as Zr, Ti, P, Y, or Nb, which are considered to be immobile during low-grade metamorphic processes (e.g. Floyd and Winchester, 1975, 1978; Herrmann et al., 1974). The majority of the samples plot into the field of WPB (within-plate basalts) within a Zr–Zr/Y diagram (Fig. 9A - Pearce and Norry, 1979). Moreover, the connection to the intra-plate magmatism is supported by both low Th/Ta ratios (~5.35) and low Yb contents (~4.51 ppm), as well as distinctive Ta/Yb (~0.45) and Th/Yb (~2.40) ratios - the above features are peculiar to WPVZ

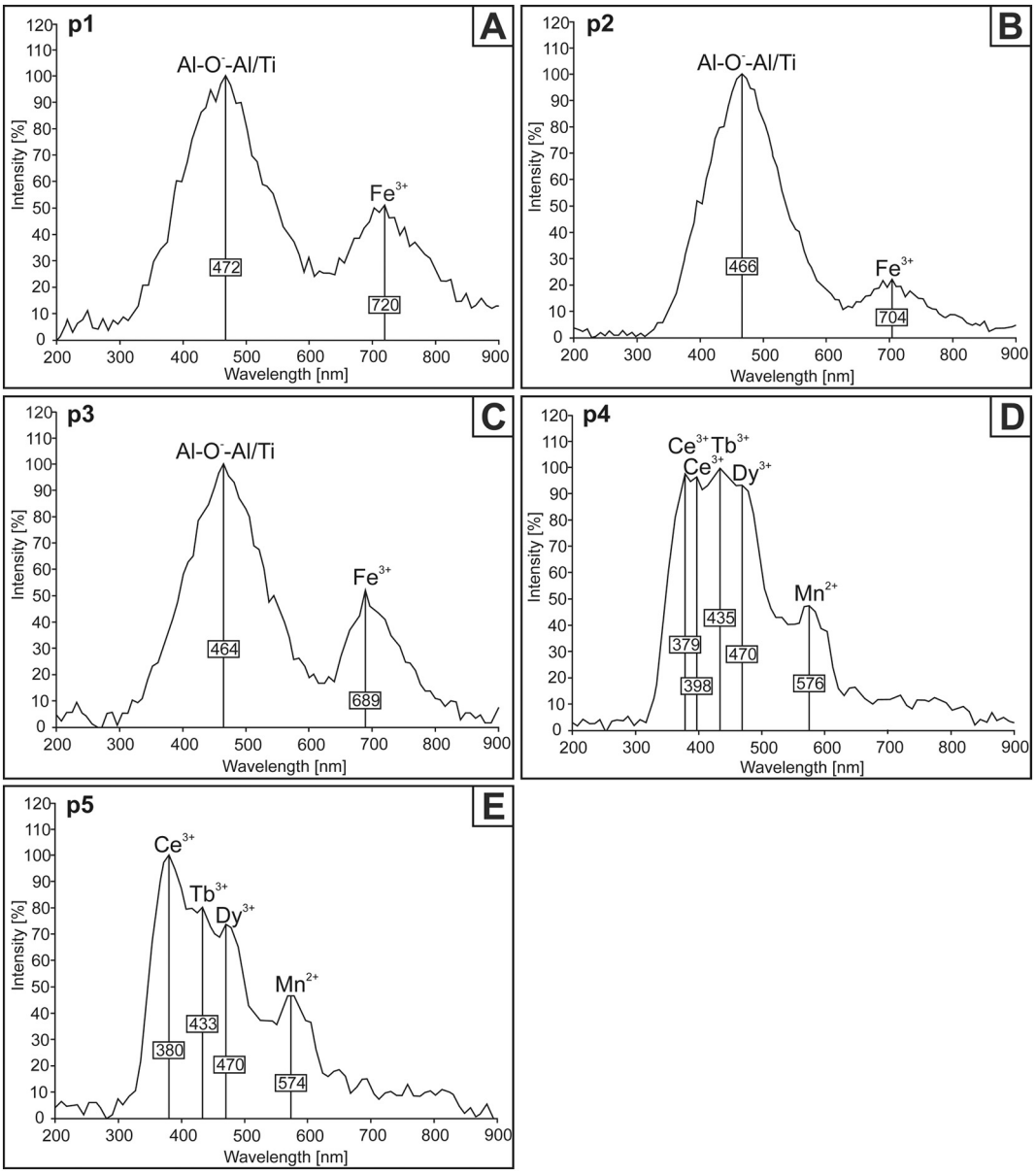

Fig. 6. SEM-CL spectra of feldspar-group minerals (A-C) including greenish-grey luminescent andesine (A; point 1 on Fig. 5A), bright-blue Ab-rich (B; point 2 on Fig. 5A) and dull-blue Or-rich (C; point 3 on Fig. 5A) alkali-feldspars; SEMCL spectra of fluoroapatite (D-E) including pink-violet luminescent (D; point 4 on Fig. 5D) and yellowish-luminescent crystals (E; point 5 on fig. 5D).

(within-plate volcanic zones) according to Gorton and Schandl (2000) and Pearce (1983), respectively. The samples are characterised by high Nb/Yb (~7.96) and Th/Yb (~2.40) ratios compared to MORB, which is typical of active continental margins (epicontinental arcs) and/or suggests an involvement of crustal material during rock formation (Pearce, 2008) - Fig. 9B. Based on the distribution of 2Nb–Zr/4–Y we further infer that the trachyandesites were emplaced as within-plate alkali basalts (Meschede, 1986) - Fig. 9C. On the contrary, the position of the samples within Hf/3–Th–Ta diagram point to the settings typical of volcanic-arc alkaline basalts (Wood, 1980) - Fig. 9D. Arc-related affinities are also evidenced by significant enrichment in LILE (e.g. Rb, Ba) and LREE (La—Sm) as well as relatively low Th/La (~0.14) ratios (e.g. Xu et al., 2017).

Overall, the formation of the intra-continental magmas, which are typical of the Intra-Sudetic Basin (e.g. Awdankiewicz, 1999a, 1999b), could be explained by such petrotectonic models as: (1) crustal contamination via assimilation and fractional crystallization (AFC model - Dupuy and Dostal, 1984), (2) the involvement of subduction modified (possibly metasomatised) lithospheric mantle (Dostal et al., 1989), and/or (3) mafic replenishment of the magma chamber (Hogg et al., 1989). Strong depletion in Cr and Ni, related to the advanced fractional crystallization of ferromagnesian minerals/Fe-Ti oxides, possibly preclude the presence of the mafic replenishment (cf. Awdankiewicz, 2006). High La/Nb (~2.24), La/Ta (~39.65), and Ba/La (~11.22)[1] ratios further suggest enriched (subduction-modified) subcontinental mantle source of the melts (Saunders et al., 1992; Thompson and Morrison, 1988). Regarding extension-related post-collisional settings of volcanites from the Intra-Sudetic Basin (Awdankiewicz, 1999a, 1999b), the subduction-related features were likely imparted by the previous tectonic events of the Variscan orogeny preceding Early-Permian magmatic activity in the study area. Hence, the preservation of both within-plate and arc-like signatures is observed among investigated

[1] Only weakly altered samples were concerned due to high variations of BaO content resulting from a secondary alteration

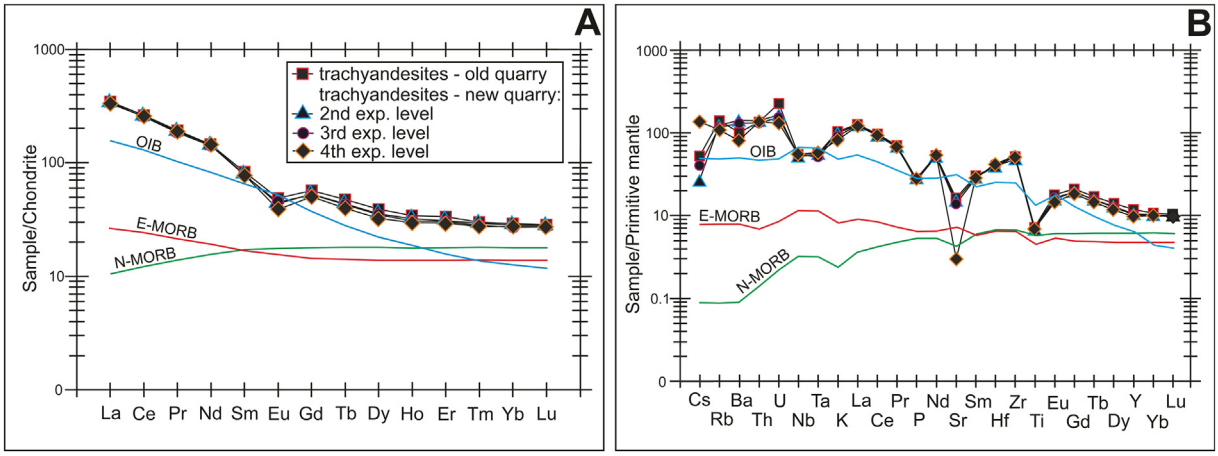

Fig. 7. Chondrite-normalized REE patterns (A) and primitive mantle-normalized multi-element spider diagrams (B) for trachyandesites from Świerki quarry (mean data for two samples per exposure level) (normalization values after McDonough and Sun, 1995).

samples. Similar conclusions were made by Awdankiewicz (2006) who studied the petrology of continental Permian volcanites from the North-Sudetic Basin. These rocks reveal a comparable geochemical features as those examined in this study.

The comparison of the chemical composition of the rocks with primitive mantle composition revealed a significant depletion of Nb—Ta ($[Nb/Th]_{PM}$:0.37–0.42; $[Ta/Th]_{PM}$:0.38–0.43) relative to LILE and LREE coupled with positive spikes for Zr—Hf (Fig. 7B). The samples are characterised by negative P and Ti anomalies as well as low Nb/U ratios (~10.99). They exhibit high Ti/Zr (~15.99) ratios and elevated $[Th/Yb]_{PM}$ values in the range of 12.45–14.18 (Fig. 9B). Therefore, we infer that the parental magmas of trachyandesites from Świerki quarry were most probably affected by some crustal input (contamination) during their evolution (see: Fan and Kerrich, 1997; Wilson, 1989; Zhang et al., 2007; Zhang et al., 2009; Zhao et al., 2010; Zhao and Zhou, 2007).

The minor Eu anomalies observed in trachyandesites from Świerki quarry point to a negligible role of plagioclase fractionation. The low Mg# values (< 40) in the least altered samples alongside with low Cr and Ni content indicate the magma was significantly evolved.

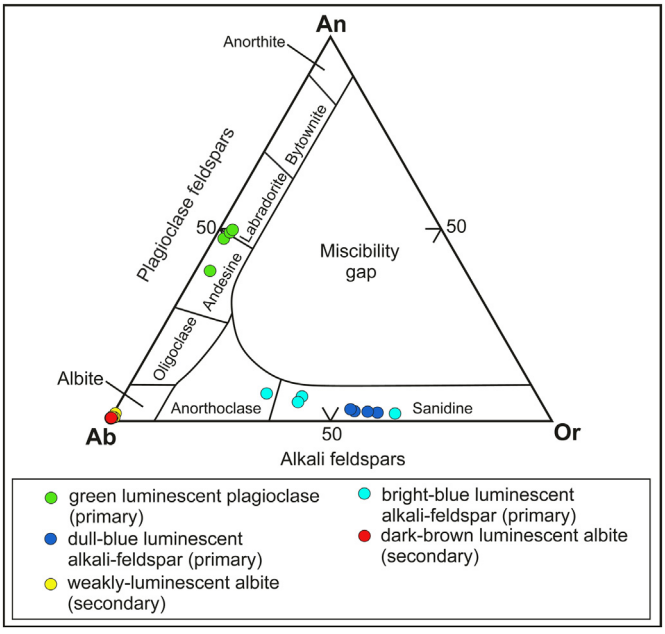

Fig. 8. An-Ab-Or ternary plot showing composition and classification of plagioclases and alkali-feldspars as well as secondary albites based on combined electron microprobe analyses (EMPA) and cathodoluminescence microscopy (OM-CL).

5.5. The effects of spilitization on main and trace element distribution

According to Hellmann et al. (1979 - see also: Floyd, 1977; Hövelmann et al., 2010) not only is the composition of main elements susceptible to low-grade metamorphic processes (e.g. K or Na-related metasomatism), but also the content of REE (especially LREE) may be significantly modified by chloritization, albitization, and carbonatization processes. Consequently, it may be hard to distinguish if the REE patterns of spilitized rocks are of primary or secondary origin. Although the alteration degree varies among the investigated samples, the REE concentrations are suggested to be of a magmatic origin, as they occur in a narrow range and are not remarkably correlated with parameters reflecting various alteration degrees, i.e. L.O.I or Rb/Sr and CaO/Na_2O ratios. The transition elements (e.g. Cr, Ni, Ti) and HFSE (e.g. Nb, Ta, Zr, Hf) were also immobile during secondary alteration. LILE elements including Sr, Cs, and Ba have likely undergone some redistribution, whereas concentration of Rb has not been significantly modified (Fig. 10). What is more, although strongly altered samples are enriched in secondary albite, no significant increase of Na_2O in the whole-rock analysis is being observed.

The distribution of spilitization processes within the magmatic body from Świerki quarry was discussed by Dziedzicowa (1958) and Nowakowski (1968), who noted that alteration developed unevenly in the magmatic body and locally tended to increase towards the upper parts of the quarry. On the basis of the main and trace element distribution, the samples from the highest levels of the new quarry present the highest degree of alteration. This observation is consistent with combined SEM-EDS and CL observations, which revealed the presence of pervasive albitization in the rocks from the 4th exploitation levels of the quarry. The strongly altered samples (MD-SP7–8) have relatively low CaO/Na_2O ratios (ca. 0.71) and normative anorthite content (ca. 15%), while their Rb/Sr ratio is as high as ca. 1.06. Furthermore, their low Sr and high Cs contents compared to the rest of the samples seem to be directly connected with spilitization processes. The depletion in Sr is linked to the removal of Ca from plagioclases during albitization. The increase of Cs content may be in turn explained by crystallization of low-temperature products such as chlorite that frequently accompanies completely albitized andesines or labradorites.

6. Conclusions

Our study provided insights into the evolution of the Early-Permian trachyandesites from Świerki quarry found in the central part the Intra-Sudetic Basin (Lower Silesia, Poland). The major conclusions are as follows:

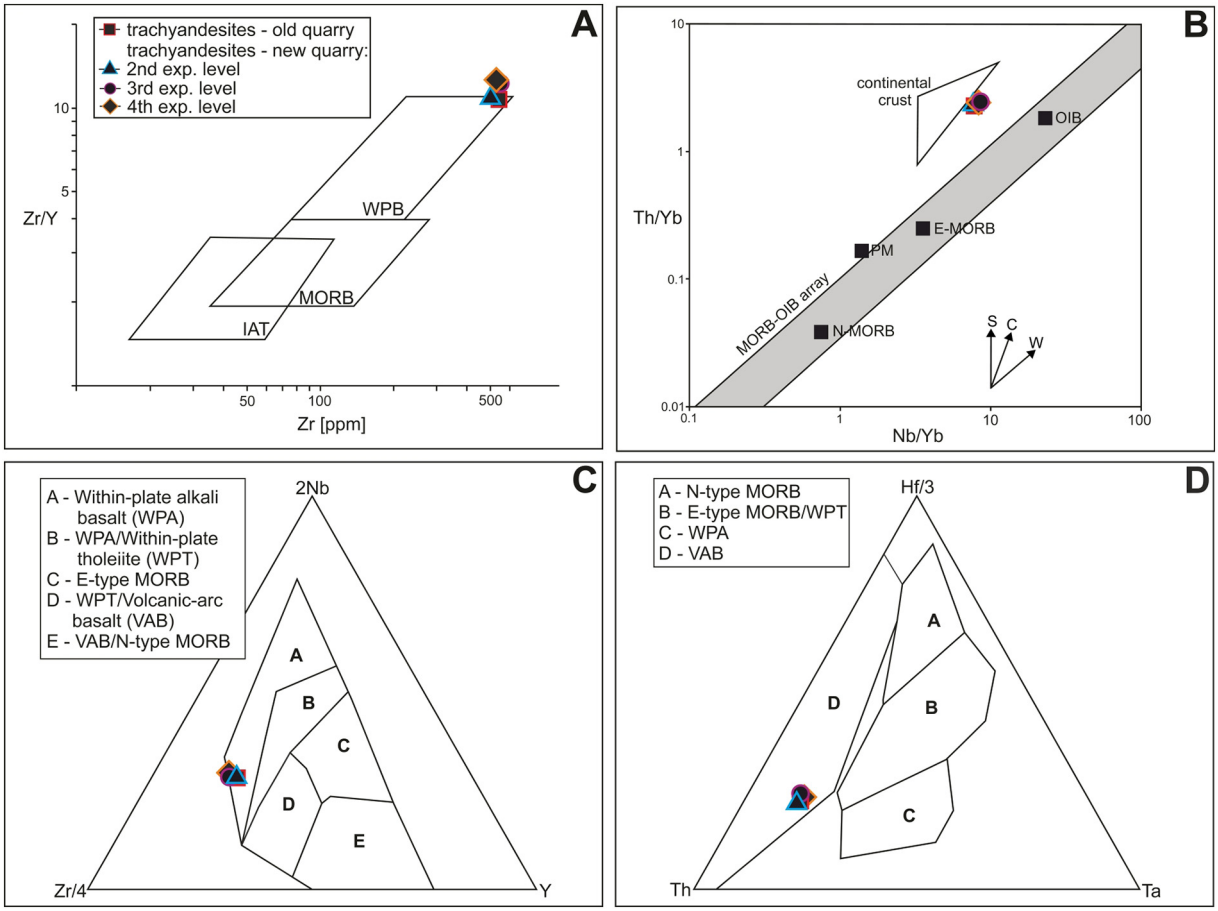

Fig. 9. Tectonomagmatic discrimination diagrams for trachyandesites from Świerki quarry. (A) Zr/Y vs. Zr diagram (after Pearce and Norry, 1979); (B) Nb/Yb–Th/Yb discrimination diagram (after Pearce, 2008) - S, C, and W are vectors for involvement of subduction component, crustal contamination, and within-plate enrichment, respectively; (C) 2Nb–Zr/4–Y diagram (after Meschede, 1986); (D) Hf/3–Th–Ta diagram (after Wood, 1980).

(1) Trachyandesites were emplaced as within plate basalts, but also carry the signature typical of arc-related volcanites. The parent magmas of the rocks were possibly derived from the enriched lithospheric mantle source (i.e. high La/Nb and La/Ta ratios and low Th/La ratios) suggesting that post-collisional magmatic activity form the Intra-Sudetic Basin has possibly inherited subduction-related geochemical affinities of previous tectonic events of the Variscan orogeny. Nevertheless, the contribution of crustal contamination to the rock evolution is highly presumable due to i.e. low Nb/U ratios and enrichment in Zr and Hf.

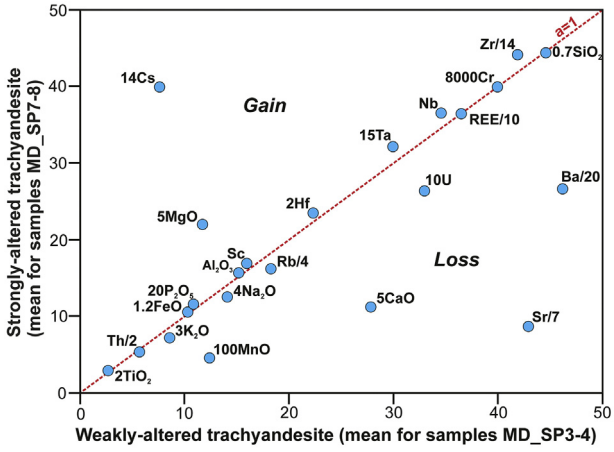

Fig. 10. Isocon diagram showing relative gain and loss of selected major and trace elements between strongly-altered and weakly-altered samples assuming there was no volume change during metasomatism. Chemical constituents gained during secondary alteration (spilitization) generally plot above the a = 1 line, whereas those lost during spilitization fall below this line. Arbitrary scaling factors were added to some elements.

(2) The so-called spilite reaction, which was responsible for the formation of albite at the expense of primary plagioclases (andesine-labradorite), was triggered by crystallographically-controlled, interface-coupled dissolution-reprecipitation mechanism. The newly-formed secondary albite exhibits pure chemical composition and weakly luminescent to dark-brown luminescent character.

(3) The spilitization had minor effects on redistribution of trace elements, in particular LREE and HREE. In contrast, the alteration processes contributed to the significant decrease of Sr and increase of Cs concentration, linked to the pervasive albitization accompanied by chloritization.

(4) There is a positive correlation between TiO_2 and BaO content with the intensity of blue CL colours among alkali-feldspars from the rocks. Hence, not only was the origin of blue luminescence colours ascribed to the coupled KSi-BaAl substitution and associated
Al-O-Al-related defects, but also Ti^{4+} impurity should be considered as potential activator in this group of minerals.

Acknowledgements

The authors would like to thank Leszek Giro for making CL spectroscopy. We sincerely thank Jarosław Majka for his valuable suggestions

during manuscript preparation. Adam Włodek is thanked for his help during EMP analyses. Anonymous reviewers are acknowledged for their friendly and critical comments that helped to significantly improve the manuscript. This study was supported by research statutory grant no 11.11.140.158 from the AGH University of Science and Technology (Krakow, Poland).

Disclosure statement

No potential conflict of interest was reported by the authors.

References

Amstutz, G.C. (Ed.), 1974. Spilites and Spilitic Rocks. Springer-Verlag, Berlin, Heidelberg.
Andersen, D.J., Lindsley, D.H., 1985. New (and Final!) Models for the Ti-Magnetite/Ilmenite Geothermometer and Oxygen Barometer. Eos, Transactions. Vol. 66. American Geophysical Union.
Árkai, P., Sassi, F.P., Desmons, J., 2007. A Systematic Nomenclature for Metamorphic Rocks: 5. Very Low- to Low-Grade Metamorphic Rocks. Recommendations by the IUGS Subcommission on the Systematics of Metamorphic Rocks, pp. 1–12.
Awdankiewicz, M., 1999a. Volcanism in a late Variscan intramontane trough: Carboniferous and Permian volcanic centres of the Intra-Sudetic Basin, SW Poland. Geologia Sudetica 32, 13–47.
Awdankiewicz, M., 1999b. Volcanism in a late Variscan intramontane trough: the petrology and geochemistry of the Carboniferous and Permian volcanic rocks of the Intra-Sudetic Basin SW Poland. Geologia Sudetica 32, 83–111.
Awdankiewicz, M., 2004. Sedimentation, volcanism and subvolcanic intrusions in a late Palaeozoic intramontane trough (the Intra-Sudetic Basin, SW Poland). Geological Society, London, Special Publications 234, 5–11.
Awdankiewicz, M., 2006. Fractional Crystallization, Mafic Replenishment and Assimilation in crustal magma chambers: geochemical constraints from the Permian post-collisional intermediate-composition volcanic suite of the North-Sudetic Basin (SW Poland). Geologia Sudetica 38, 39–61.
Awdankiewicz, M., Kurowski, L., Mastalerz, K., Raczyński, P., 2003. The Intra-Sudetic Basin - a record of sedimentary and volcanic processes in late to post-Orogenic tectonic setting. GeoLines 16, 165–183.
Baker, L.L., Rember, W.C., Sprenke, K.F., Strawn, D.G., 2012. Celadonite in continental flood basalts of the Columbia River Basalt Group. American Mineralogist 97, 1284–1290.
Betsi, T.B., Lentz, D.R., 2010. The nature of "quartz eyes" hosted by dykes associated with Au-Bi-As-Cu, Mo-Cu, and Base-metal-Au-Ag mineral occurrences in the Mountain Freegold region (Dawson Range), Yukon, Canada. Journal of Geosciences 55, 347–368.
Birkenmajer, K., Grocholski, A., Milewicz, J., Nairn, A.E.M., 1968. Palaeomagnetic studies of polish rocks II. The upper Carboniferous and lower Permian of the Sudetes. Annales Societatis Geologorum Poloniae 38, 435–474.
Brongniart, A., 1827. Classification et caractères minéralogiques des roches homogènes et hétérogènes. F.G. Levrault (in French).
Brown, W.L., 1993. Fractional crystallization and zoning in igneous feldspars: ideal water-buffered liquid fractionation lines and feldspar zoning paths. Contributions to Mineralogy and Petrology 113, 115–125.
Buddington, A.F., Lindsley, D.H., 1964. Iron-titanium oxide minerals and synthetic equivalents. Journal of Petrology 5, 310–357.
Coombs, D.S., 1974. On the mineral facies of spilitic rocks and their genesis. In: Amstutz, G. C. (Ed.), Spilites and Spilitic Rocks. Springer-Verlag, Berlin, Heidelberg, pp. 373–380.
Davies, J.F., Grant, R.W.E., Whitehead, R.E.S., 1979. Immobile trace elements and Archaean volcanic stratigraphy in the Timmins mining areas, Ontario. Canadian Journal of Earth Sciences 16, 305–311.
Dostal, J., Wilson, R.A., Keppie, J.D., 1989. Geochemistry of Siluro-Devonian Tobique volcanic belt in northern and Central New Brunswick (Canada): Tectonic implications. Canadian Journal of Earth Sciences 26, 1282–1296.
Dupuy, C., Dostal, J., 1984. Trace element geochemistry of some continental tholeiites. Earth and Planetary Science Letters 67, 61–69.
Dziedzic, K., 1958. The succession of Permian volcanic rocks in the vicinity of Nowa Ruda (lower Silesia, Poland). Annales Societatis Geologorum Poloniae 28, 109–120 (in Polish with English summary).
Dziedzicowa, H., 1958. The metasomatism of Permian "melaphyre" from Świerki village (lower Silesia, Poland). Annales Societatis Geologorum Poloniae 79-107, 28 (in Polish with English summary).
Engvik, A.K., Putnis, A., Gerald, J.D.F., Austrheim, H., 2008. Albitization of granitic rocks: the mechanism of replacement of oligoclase by albite. The Canadian Mineralogist 46, 1401–1415.
Eskola, P., Vuoristo, U., Rankama, K., 1937. An experimental illustration of the spilite reaction. Bulletin of the Geological Society of Finland (119), 61–68.
Fan, J., Kerrich, R., 1997. Geochemical characteristics of aluminum depleted and undepleted komatiites and HREE-enriched low-Ti tholeiites, western Abitibi greenstone belt: a heterogeneous mantle plume-convergent margin environment. Geochimica et Cosmochimica Acta 61, 4723–4744.
Fedo, C.M., Young, G.M., Nesbitt, H.W., Hanchar, J.M., 1997. Potassic and sodic metasomatism in the southern province of the Canadian Shield: evidence from the Paleoproterozoic Serpent Formation, Huronian Supergroup, Canada. Precambrian Research 84, 17–36.
Finch, A.A., Klein, J., 1999. The causes and petrological significance of cathodoluminescence emissions from alkali feldspars. Contributions to Mineralogy and Petrology 135, 234–243.
Floyd, P.A., 1977. Rare earth element mobility and geochemical characterisation of spilitic rocks. Nature 269, 134–137.
Floyd, P.A., Winchester, J.A., 1975. Magma type and tectonic setting discrimination using immobile elements. Earth and Planetary Science Letters 27, 211–218.
Floyd, P.A., Winchester, J.A., 1978. Identification and discrimination of altered and metamorphosed volcanic rocks using immobile elements. Chemical Geology 21, 291–306.
Franke, W., Żelaźniewicz, A., 2000. The eastern termination of the Variscides: terrane correlation and kinematic evolution. Geological Society, London, Special Publications 179, 63–86.
Fu, J.Q., Wang, C.S., 1984. The statistic analyses of ca/Na ratios in classification of spilites. Geology-Geochemistry 10, 55–56 (in Chinese with English abstract).
Garcia, M.O., 1978. Criteria for the identification of ancient volcanic arcs. Earth-Science Reviews 14, 147–165.
Geuna, S.E., Lagorio, S.L., Vizan, H., 2014. Oxidation processes and their effects on the magnetic remanence of early cretaceous subaerial basalts from Sierra Chica de Córdoba, Argentina. Geological Society, London, Special Publications 396, SP396–13.
González-Acebrón, L., Götze, J., Barca, D., Arribas, J., Mas, R., Pérez-Garrido, C., 2012. Diagenetic albitization in the Tera Group, Cameros Basin (NE Spain) recorded by trace elements and spectral cathodoluminescence. Chemical Geology 312, 148–162.
Gorton, M.P., Schandl, E.S., 2000. From continents to island arcs: a geochemical index of tectonic setting for arc-related and within-plate felsic to intermediate volcanic rocks. The Canadian Mineralogist 38, 1065–1073.
Götze, J., 2012. Application of cathodoluminescence microscopy and spectroscopy in geosciences. Microscopy and Microanalysis 18, 1270–1284.
Götze, J., Krbetschek, M.R., Habermann, D., Wolf, D., 2000. High-resolution cathodoluminescence studies of feldspar minerals. In: Pagel, M., Barbin, V., Blanc, P., Ohnenstetter, D. (Eds.), Cathodoluminescence in Geosciences. Springer-Verlag, Berlin Heidelberg, pp. 245–270.
Guo, J., Green, T.H., 1989. Barium partitioning between alkali feldspar and silicate liquid at high temperature and pressure. Contributions to Mineralogy and Petrology 102, 328–335.
Habermann, D., Neuser, R.D., Richter, D.K., 2000. Quantitative high resolution spectral analysis of Mn^{2+} in sedimentary calcite. In: Pagel, M., Barbin, V., Blanc, P., Ohnenstetter, D. (Eds.), Cathodoluminescence in Geosciences. Springer-Verlag, Berlin Heidelberg, pp. 331–358.
Haggerty, S.E., 1991. Oxide textures - a mini-atlas. In: Lindsley, D.H. (Ed.), Oxide Minerals: Petrologic and Magnetic Significance. Vol. 25. Mineralogical society of America, pp. 129–220.
Hall, A., 1990. Geochemistry of spilites from South-West England: a statistical approach. Mineralogy and Petrology 41, 185–197.
Heflik, W., Pawlikowski, M., 1977. Jaspers from Świerki Village (Lower Silesia, Poland). Przegląd Geologiczny. vol. 25, pp. 239–243 (in Polish with English summary).
Hellman, P.L., Smith, R.E., Henderson, P., 1979. The mobility of the rare earth elements: evidence and implications from selected terrains affected by burial metamorphism. Contributions to Mineralogy and Petrology 71, 23–44.
Herrmann, A.G., Potts, M.J., Knake, D., 1974. Geochemistry of the rare earth elements in spilites from the oceanic and continental crust. Contributions to Mineralogy and Petrology 44, 1–16.
Hogg, A.J., Fawcett, J.J., Gittins, J., Gorton, M.P., 1989. Cyclical variation in composition in continental tholeiites of East Greenland. Canadian Journal of Earth Sciences 26, 534–543.
Holub, V.M., 1976. Permian Basins in the Bohemian Massif. In: Falke, H. (Ed.), The Continental Permian in Central, West, and South Europe. Springer, Netherlands, pp. 53–79.
Hövelmann, J., Putnis, A., Geisler, T., Schmidt, B.C., Golla-Schindler, U., 2010. The replacement of plagioclase feldspars by albite: observations from hydrothermal experiments. Contributions to Mineralogy and Petrology 159, 43–59.
Kastner, M., 1971. Authigenic feldspars in carbonate rocks. American Mineralogist: Journal of Earth and Planetary Materials 56, 1403–1442.
Kayama, M., Nakano, S., Nishido, H., 2010. Characteristics of emission centers in alkali feldspar: a new approach by using cathodoluminescence spectral deconvolution. American Mineralogist 95, 1783–1795.
Kempe, U., Götze, J., 2002. Cathodoluminescence (CL) behaviour and crystal chemistry of apatite from rare-metal deposits. Mineralogical Magazine 66, 151–172.
Kontonikas-Charos, A., Ciobanu, C.L., Cook, N.J., Ehrig, K., Krneta, S., Kamenetsky, V.S., 2017. Feldspar evolution in the Roxby Downs Granite, host to Fe-oxide Cu-Au-(U) mineralisation at Olympic Dam, South Australia. Ore Geology Reviews 80, 838–859.
Kozłowski, S., 1958. Permian Volcanism in the Area of Głuszyca and Świerki (Lower Silesia, Poland). Annales Societatis Geologorum Poloniae. vol. 28, pp. 5–61 (in Polish with English summary).
Kozłowski, S., 1963. The geology of Permian volcanic rocks from the central part of Intra-Sudetic basin (lower Silesia, Poland). Prace Geologiczne Komisji Nauk Geologicznych PAN (Oddział w Krakowie). Wydawnictwa Geologiczne, Warszawa (in Polish with English summary).
Krbetschek, M.R., Götze, J., Irmer, G., Rieser, U., Trautmann, T., 2002. The red luminescence emission of feldspar and its wavelength dependence on K, Na, Ca – composition. Minerals and Petroleum 76, 167–177.
Lawrence, M.G., Greig, A., Collerson, K.D., Kamber, B.S., 2006. Rare earth element and yttrium variability in South East Queensland waterways. Aquatic Geochemistry 12, 39–72.
Lee, M.R., Parsons, I., Edwards, P.R., Martin, R.W., 2007. Identification of cathodoluminescence activators in zoned alkali feldspars by hyperspectral imaging and electron-probe microanalysis. American Mineralogist 92, 243–253.

Lefleche, M.R., Dupuy, C., Bougault, H., 1992. Geochemistry and petrogenesis of Archean volcanic rocks of the southern Abitibi Belt, Quebec. Precambrian Research 57, 207–241.
Lehmann, E., 1974a. Spilitic magma. Characteristics and mode of formation. In: Amstutz, G.C. (Ed.), Spilites and Spilitic Rocks. Springer-Verlag, Berlin Heidelberg, pp. 23–38.
Lehmann, E., 1974b. Environmental Effects in Magmatic Spilite. In: Amstutz, G.C. (Ed.), Spilites and Spilitic Rocks. Springer-Verlag, Berlin Heidelberg, pp. 113–126.
Leichmann, J., Broska, I., Zachovalova, K., 2003. Low-grade metamorphic alteration of feldspar minerals: a CL study. Terra Nova 15, 104–108.
Lorenz, V., Nicholls, I.A., 1976. The permocarboniferous basin and range province of Europe. An application of plate tectonics. In: Falke, H. (Ed.), The Continental Permian in Central, West and South Europe. Springer, Netherlands, pp. 313–342.
Machel, H.G., Mason, R.A., Mariano, A.N., Mucci, A., 1991. Causes and emission of luminescence in calcite and dolomite. In: Barker, C.E., Kopp, O.C. (Eds.), Luminescence Microscopy and Spectroscopy - Qualitative and quantitative applications. SEPM (Society for Sedimentary Geology) Short Course, No. 25, pp. 9–25.
MacLean, W.H., Barrett, T.J., 1993. Lithochemical techniques using immobile elements. Journal of Geochemical Exploration 48, 109–133.
Marfunin, A.S., 1979. Spectroscopy, Luminescence and Radiation Centers in Minerals. Springer-Verlag, Berlin, Heidelberg.
Mariano, A.N., 1988. Some further geological applications of cathodoluminescence. In: Marshall, D.J. (Ed.), Cathodoluminescence of Geological Materials. Unwin Hyman, Boston, pp. 94–123.
Mariano, A.N., Ito, J., Ring, P.J., 1973. Cathodoluminescence of plagioclase feldspars. Geological Society of America, p. 726 Abstract Program 5.
McCann, T. (Ed.), 2008. The Geology of Central Europe. Geological Society of London, London.
McDonough, W.F., Sun, S.S., 1995. The composition of the Earth. Chemical Geology 120, 223–253.
Mengel, K., Borsuk, A.M., Gurbanov, A.G., Wedepohl, K.H., Baumann, A., Hoefs, J., 1987. Origin of spilitic rocks from the southern slope of the Greater Caucasus. Lithos 20, 115–133.
Meschede, M., 1986. A method of discriminating between different types of mid-ocean ridge basalts and continental tholeiites with the Nb-Zr-Y diagram. Chemical Geology 56, 207–218.
Mora, C.I., Ramseyer, K., 1992. Cathodoluminescence of coexisting plagioclases, Boehls Butte anorthosite: CL activators and fluid flow paths. American Mineralogist 77, 1258–1265.
Mücke, A., 2003. Magnetite, ilmenite and ulvite in rocks and ore deposits: petrography, microprobe analyses and genetic implications. Mineralogy and Petrology 77, 215–234.
Munhá, J., Kerrich, R., 1980. Sea water basalt interaction in spilites from the Iberian Pyrite Belt. Contributions to Mineralogy and Petrology 73, 191–200.
Narebski, W., Dostal, J., Dupuy, C., 1986. Geochemical characteristics of lower Paleozoic spilite-keratophyre series in the Western Sudetes (Poland): petrogenetic and tectonic implications. Neues Jahrbuch für Mineralogie 155, 243–258 Abhandlungen.
Nowakowski, A., 1968. Permian volcanic rocks from Suche Mts. Range in Intra-Sudetic Basin. Geologia Sudetica 4, 299–408 (in Polish with English summary).
Odin, G.S., Desprairies, A., Fullgar, P.D., Bellon, H., Decarreau, A., Fröhlich, F., Zelvelder, M., 1988. Nature and geological significance of celadonite. In: Odin, G.S. (Ed.), Green Marine Clays: Oolitic Ironstone Facies, Verdine Facies, Glaukony Facies and Celadonite-Bearing Rock Facies - a Comparative Study. Elsevier, Amsterdam, pp. 337–392.
Orlický, O., 2010. On the demonstration of the normal polarity of remanent magnetization by volcanic rocks containing magnetite or hematite. Contributions to Geophysics and Geodesy 40, 263–282.
Parsons, I., Steele, D.A., Lee, M.R., Magee, C.W., 2008. Titanium as a cathodoluminescence activator in alkali feldspars. American Mineralogist 93, 875–879.
Pearce, J.A., 1983. Role of the sub-continental lithosphere in magma genesis at active continental margins. In: Hawkesworth, C.J., Norry, M.J. (Eds.), Continental Basalts and Mantle Xenoliths. Shiva Press, Nantwich, pp. 230–249.
Pearce, J.A., 2008. Geochemical fingerprinting of oceanic basalts with applications to ophiolite classification and the search for Archean oceanic crust. Lithos 100, 14–48.
Pearce, J.A., Norry, M.J., 1979. Petrogenetic implications of Ti, Zr, Y, and Nb variations in volcanic rocks. Contributions to Mineralogy and Petrology 69, 33–47.
Plümper, O., Putnis, A., 2009. The complex hydrothermal history of granitic rocks: multiple feldspar replacement reactions under subsolidus conditions. Journal of Petrology 50, 967–987.
Putnis, A., 2002. Mineral replacement reactions: from macroscopic observations to microscopic mechanisms. Mineralogical Magazine 66, 689–708.
Que, M., Allen, A.R., 1996. Sericitization of plagioclase in the Rosses granite complex, Co. Donegal, Ireland. Mineralogical Magazine 60, 927–936.
Ramseyer, K., Baumann, J., Matter, A., Mullis, J., 1988. Cathodoluminescence colours of alpha quartz. Mineralogical Magazine 52, 669–677.
Ramseyer, K., Boles, J.R., Lichtner, P.C., 1992. Mechanism of plagioclase albitization. Journal of Sedimentary Research 62, 349–356.
Richter, D.K., Götte, T., Habermann, D., 2002. Cathodoluminescence of authigenic albite. Sedimentary Geology 150, 367–374.
Saunders, A.D., Storey, M., Kent, R.W., Norry, M.J., 1992. Consequences of plume– lithosphere interactions. In: Storey, B.C., Alabaster, T., Pankhurst, R.J. (Eds.), Magmatism and the Cause of Continental Breakup. vol. 68. Geological Society of Special Publication, London, pp. 41–60.
Słaby, E., Götze, J., 2004. Feldspar crystallization under magma-mixing conditions shown by cathodoluminescence and geochemical modelling - a case study from the Karkonosze pluton (SW Poland). Mineralogical Magazine 68, 561–577.
Słaby, E., Götze, J., Wörner, G., Simon, K., Wrzalik, R., Śmigielski, M., 2008. K-feldspar phenocrysts in microgranular magmatic enclaves: a cathodoluminescence and geochemical study of crystal growth as a marker of magma mingling dynamics. Lithos 105, 85–97.
Smith, R.E., 1968. Redistriution of Major elements in the Alteration of some Basic Lavas during Burial Metamorphism. Journal of Petrology 9, 191–219.
Smith, J.V., Brown, W.L., 1988. Feldspar Minerals. 1. Crystal Structures, Physical, Chemical, and Microtextural Properties. Springer-Verlag, Berlin.
Speit, B., Lehmann, G., 1982. Radiation defects in feldspars. Physics and Chemistry of Minerals 8, 77–82.
Stille, H., 1950. Der "subsequente" Magmatismus. Akademie-Verlag, Berlin (in Deutsch).
Thompson, R.N., Morrison, M.A., 1988. Asthenospheric and lower-lithospheric mantle contributions to continental extension magmatism: an example from the British Tertiary Province. Chemical Geology 68, 1–15.
Turner, F.J., 1948. Mineralogical and structural evolution of the metamorphic rocks. Vol. 30. Geological Society of America.
Viswanathan, K., Kielhorn, H.M., 1983. Al,Si distribution in a ternary (Ba,K,Na)-feldspar as determined by crystal structure refinement. American Mineralogist 68, 122–124.
Vozár, J., 1974. Comments on spilitization of the Permian eruptive rocks of the Choč Nappe in the West Carpathians, Slovakia. In: Amstutz, G.C. (Ed.), Spilites and spilitic rocks. Springer-Verlag, Berlin Heidelberg, pp. 359–362.
Wendler, J., Köster, J., Götze, J., Kasch, N., Zisser, N., Kley, J., Pudlo, D., Nover, G., Gaupp, R., 2012. Carbonate diagenesis and feldspar alteration in fracture-related bleaching zones (Buntsandstein, Central Germany): possible link to CO_2-influenced fluid-mineral reactions. International Journal of Earth Sciences 101, 159–176.
White, W.B., Masako, M., Linnehan, D.G., Fukukawa, T., Chandrasekhar, B.K., 1986. Absorption and luminescence of Fe^{3+} in single crystal orthoclase. American Mineralogist 71, 1415–1419.
Wilson, M., 1989. Igneous Petrogenesis. Unwin Hyman Ltd, London.
Winchester, J.A., Floyd, P.A., 1977. Geochemical discrimination of different magma series and their differentiation products using immobile elements. Chemical Geology 20, 325–343.
Wojewoda, J., Mastalerz, K., 1989. Climate evolution, anocyclicity, and autocyclity of sedimentations based on continental sediments of upper Carboniferous and Permian in Sudetes. Przegląd Geologiczny 37, 173–179 (in Polish with English summary).
Wood, D.A., 1980. The application of a Th-Hf-Ta diagram to problems of tectonomagmatic classification and to establishing the nature of crustal contamination of basaltic lavas of the British Tertiary Volcanic Province. Earth and Planetary Science Letters 50, 11–30.
Xia, L., Xia, Z., Ren, Y., Peng, L., Zhang, C., Yang, J., Wang, X., Li, Z., Han, S., Huang, Z., 1991. Marine Volcanic Rocks from Qilian and Qinling Mountains. China University of Geosciences Press, Wuhan (in Chinese with English abstract).
Xing, C.M., Wang, C.Y., 2017. Cathodoluminescence images and trace element compositions of fluorapatite from the Hongge layered intrusion in SW China: a record of prolonged crystallization and overprinted fluid metasomatism. American Mineralogist 102, 1390–1401.
Xu, W., Xu, X., Zeng, G., 2017. Crustal contamination versus an enriched mantle source for intracontinental mafic rocks: Insights from early Paleozoic mafic rocks of the South China Block. Lithos 286, 388–395.
Zhang, C.L., Gao, S., Yuan, H.L., Zhang, G.W., Yan, Y.X., Luo, J.L., Luo, J.H., 2007. Sr–Nd–Pb isotopes of the early Paleozoic mafic–ultra- mafic dykes and basalts from south Qinling belt and their implications for mantle composition. Science in China Series D: Earth Sciences 50, 1293–1301.
Zhang, Z., Mao, J., Chai, F., Yan, S., Chen, B., Pirajno, F., 2009. Geochemistry of the Permian Kalatongke mafic intrusions, northern Xinjiang, Northwest China. Implications for the genesis of magmatic Ni-Cu sulfide deposits. Economic Geology 104, 185–203.
Zhao, J.H., Zhou, M.F., 2007. Geochemistry of Neoproterozoic mafic intrusions in the Panzhihua district (Sichuan Province, SW China). Implications for subduction related metasomatism in the upper mantle. Precambrian Research 152, 27–47.
Zhao, J.H., Zhou, M.F., Zheng, J.P., 2010. Metasomatic mantle source and crustal contamination for the formation of the Neoproterozoic mafic dike swarm in the northern Yangtze Block, South China. Lithos 115, 177–189.